ARTICLE

TECHNOLOGY

Building an experimental model of the human body with non-physiological parameters

Joseph M. Labuz[1,2], Christopher Moraes[3], David R. Mertz[1,2], Brendan M. Leung[4,5] & Shuichi Takayama[1,2,6,7]

New advances in engineering and biomedical technology have enabled recent efforts to capture essential aspects of human physiology in microscale, *in-vitro* systems. The application of these advances to experimentally model complex processes in an integrated platform — commonly called a 'human-on-a-chip (HOC)' — requires that relevant compartments and parameters be sized correctly relative to each other and to the system as a whole. Empirical observation, theoretical treatments of resource distribution systems and natural experiments can all be used to inform rational design of such a system, but technical and fundamental challenges (e.g. small system blood volumes and context-dependent cell metabolism, respectively) pose substantial, unaddressed obstacles. Here, we put forth two fundamental principles for HOC design: inducing *in-vivo*-like cellular metabolic rates is necessary and may be accomplished *in vitro* by limiting O_2 availability and that the effects of increased blood volumes on drug concentration can be mitigated through pharmacokinetics-based treatments of solute distribution. Combining these principles with natural observation and engineering workarounds, we derive a complete set of design criteria for a practically realizable, physiologically faithful, five-organ millionth-scale ($\times 10^{-6}$) microfluidic model of the human body.

***Keywords*: Human on a Chip; Organ on a Chip; Microfluidics; Oxygen Conformance; Metabolic Scaling; *C. aceratus*.**

0. INNOVATION

An integrated experimental model of the human body (a "human-on-a-chip" or HOC) holds great promise for drug discovery, personalized medicine and basic research. Despite recent achievements in this field, substantial challenges remain in faithfully recapitulating macro human function at a micro scale. Breaking with convention, we propose that non-physiologic design parameters (e.g. low "blood" oxygen carrying capacity) can be employed to induce *in-vivo*-like HOC behavior. We apply this strategy — supported by experimental and theoretical evidence — to provide detailed design criteria for a five-organ HOC capable of matching macro human function across key criteria.

1. INTRODUCTION

Advances in micro-scale engineering, cell sourcing and culture techniques are presenting new opportunities to recapitulate key structural and functional characteristics of the human body in controlled, *in-vitro*, experimental systems. Already, organ-level devices (commonly called 'organs-on-a-chip') are quite prolific[1–3]. Efforts at devising systems-level platforms (i.e. HOCs) hold even greater promise[4–7]. Ideally, these small HOCs would predict the effects of potential drugs or toxins on the human body[8–10], significantly reducing costs associated with animal and human clinical trials in the drug discovery pipeline, clarifying mechanisms of human health and disease and introducing new opportunities in personalized medicine. However, unresolved issues in both the design and fabrication of such systems present scientists and engineers with a complex, interdependent set of problems.

Animal basal metabolic rate (BMR) has been shown to scale with animal mass raised to some power[11]. Although there remains some debate as to the exact value of the exponent[12], recent research has focused on how nutrient distribution networks generally control the relationship between organism size and metabolism[13,14]. Thus, many important physical parameters scale with organism mass (M) raised to the power of a multiple of ¼ (e.g. metabolic rate, $M^{¾}$; heart rate, $M^{-¼}$; and blood volume, M^{1}), called quarter-power scaling relationships (QPSRs). These QPSRs[6,15,16], along with order of magnitude estimates[17,18], residence time and physiologically based pharmacokinetic/pharmacodynamic (PB-PKPD) models[4,5,8,19–21], empirical allometry[22,23] and functional approaches[22–24] have all been used in the design of HOCs. Although these approaches do inform values for organ compartment size and other physiological parameters, they also present two classes of intractable problems in the design and construction of such systems. The first type of problem is purely technical in nature (e.g. the need for microfluidic systems of low circulating fluid volume, but sufficient tissue volume) and may eventually be solved by steady improvement in techniques and capabilities[2,7,18,21,22]. Fundamental problems (e.g. the context-dependent

[1]Department of Biomedical Engineering, College of Engineering and School of Medicine, University of Michigan, 2200 Bonisteel Blvd, Ann Arbor, MI 48109, USA. [2]Biointerfaces Institute, University of Michigan, 2800 Plymouth Road, North Campus Research Complex (NCRC), MI 48109, USA. [3]Department of Chemical Engineering, Faculty of Engineering, McGill University, 3610 University Street, Montreal, QC, H3A 0C5, Canada. [4]Department of Applied Oral Sciences, Faculty of Dentistry, Dalhousie University, 5981 University Ave, Halifax, Nova Scotia (NS), B3H 4R2, Canada. [5]School of Biomedical Engineering, Faculties of Medicine and Engineering, Dalhousie University, 5981 University Ave, Halifax, Nova Scotia (NS), B3H 4R2, Canada. [6]Macromolecular Science and Engineering Center, College of Engineering, University of Michigan, 2300 Hayward St., Ann Arbor, MI 48109, USA. [7]Michigan Center for Integrative Research in Critical Care, University of Michigan, Ann Arbor, MI 48109, USA. Correspondence should be addressed to S.T. (takayama@umich.edu).

Received 18 November 2016; accepted 7 March 2017; published online; doi:10.1142/S2339547817500029

change in cellular BMR), however, can only be addressed by a thoughtful and deliberate design strategy[25–28].

We propose that these challenges themselves only merit concern so far as they affect the end output of the HOC. That is, the *structure* of a $\times 10^{-6}$ HOC may assume strange and unexpected forms so long as the *function* — the cellular- and system-level behavior of the HOC — is accurate and relatable to human physiology. Therefore, discrete parts of an HOC need not necessarily be confined by conventional notions of what constitutes "normal" or "physiologic". To that end, we focus on designing a $\times 10^{-6}$ HOC capable of mimicking key *functions* of a macro human, specifically (1) cellular- and macro-scale BMRs and (2) basic pharmacokinetics. We further demonstrate how naturally-occurring biological systems may stray from structures of typical physiology (e.g. a hemoglobin-free vertebrate), yet produce species capable of adapting and surviving nonetheless. As modification of any particular system parameter necessarily affects all others, both natural and artificial design alterations demand a holistic approach. Applying these general principles, we propose specific design parameters for an HOC that is practical in terms of fluid-to-cell ratios and is a $\times 10^{-6}$ miniaturization of the human body with regard to total cell mass, yet remains a faithful model of macroscopic human physiology with regards to cellular BMR, basic pharmacokinetics and inter-organ scaling.

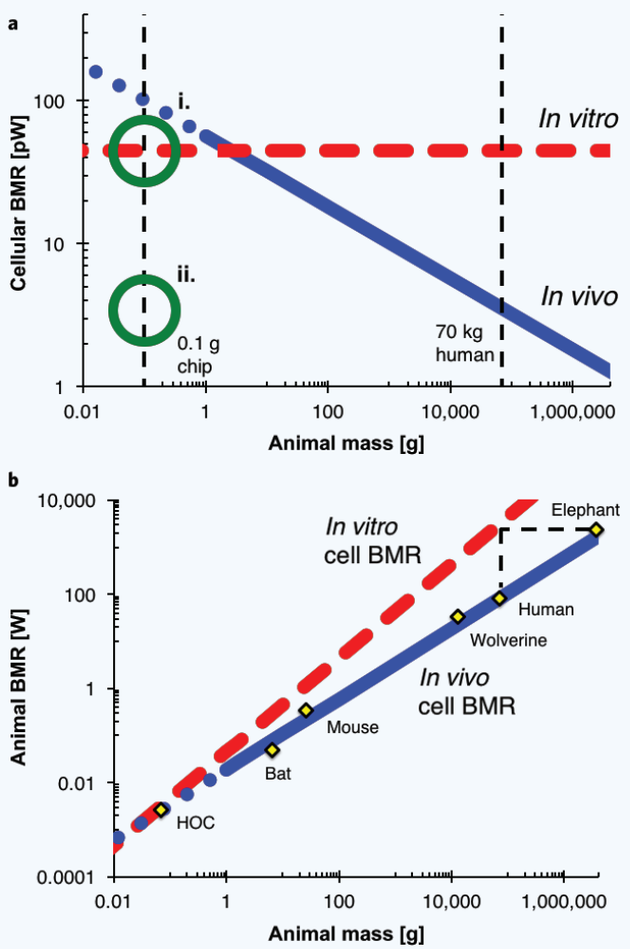

Figure 1 Consequences of context-dependent cellular basal metabolic rate (BMR). (**a**) Cellular BMR scales as $\mu M^{-1/4}$ *in vivo* but mammalian cells cultured *in vitro* have the same cellular BMR regardless of the mass of the source organism (μM^{0}). (**a-i**) *In-vitro* cell culture of human cells leads to a cellular BMR ~one order of magnitude larger than that of a normal human[25,27]. (**a-ii**) A high-fidelity, physiologically relevant human-on-a-chip (HOC) should be designed with mechanisms to ensure cellular BMR matches typical *in vivo* values for the organism to be modeled. (**b**) Failure to account for the context-dependent behavior of cells can substantially alter the modeled system BMR, especially for larger animals[25,28]. Graphs reproduced using previously published data and relationships[25,28,72].

2. CONTROL OF CELLULAR BMR

As predicted by QPSRs, cellular metabolic rate scales with animal mass[25,26,28]. However, cells cultured *in vitro* tend to operate at an elevated metabolic rate regardless of their organism of origin (**Fig. 1a**)[25,27]. Without accounting for this phenomenon, cells in an *in-vitro* HOC would have a high cellular BMR, more akin to cells in a mouse than in a human. Thus, the system BMR of the animal-on-a-chip diverges from that of the corresponding real animal; the magnitude of the error increases with animal size as $\mu M^{1/4}$ (**Fig. 1b**). For example, failure to consider the context-dependent behavior of cells in attempting to design a $\times 10^{-6}$ model of a human would result in an HOC wherein the cellular BMR is high and thus approximates that of a mouse and the system BMR is also high and approximates that of a $\times 10^{-6}$ elephant! Because of this non-linearity in scaling (i.e. M raised to a power $\neq 1$), rational design — and control — of the metabolic infrastructure of an HOC is crucial. We have previously proposed that designers must force cells in an HOC to function as they would in the macroscopic human body — that is, designers must suppress cellular BMR to match *in-vivo* levels outlined in **Fig. 1a**, in a strategy termed metabolically supported scaling[24].

Although others have demonstrated metabolic control by regulating glucose[29], ions[30], extracellular matrix (ECM) cues[31] and oxygen[24], we propose to limit O_2 availability *for the expressed purpose* of suppressing cellular BMR and inducing a more *in-vivo* like response from an HOC. Not only does this approach more closely approximate conditions in the body than the hyperoxic conditions of incubator cell culture, but *in-situ* microfluidic O_2 sensing and control is an established and active area of research[32–34]. To demonstrate that O_2 deprivation is a viable method for controlling cellular metabolic rate, we examine the behavior of human cell lines in atmospheric (20%) and physiotypic (7% and 2%) oxygen environments. Using AlamarBlue as an indicator of cellular respiration, we show that HepG2-C3A, HS-5, IMR-90 and HEK-293 cells all demonstrate significant ($p < 0.001$) oxygen conformance. A similar effect has been noted by measuring oxygen consumption rather than AlamarBlue reduction as well as predicted numerically[35,36]. As oxygen decreases, cellular metabolism follows — at physiotypic oxygen tension, cellular respiration is reduced by nearly fivefold (**Fig. 2**). Importantly, in no cases did AlamarBlue metabolism drop to zero indicating that, even after four hours culture in each O_2 atmosphere, the cells remained viable. Total cellular BMR is likely to be slightly higher than these measured values since our AlamarBlue indicator fails to respond to the anaerobic ATP production which yields ~10× less energy than aerobic processes.

Although cellular BMR saw at most a fivefold reduction, compared to the 10× theoretical difference between cells *in vivo* and *in vitro* (**Fig. 1a**), these results demonstrate that oxygen deprivation is a viable strategy for reducing cellular BMR to be more in line with "natural" levels. Moreover, the results demonstrate that cells remained viable in pO_2 up to 10× lower than a conventional cell culture incubator (perhaps unsurprising given that such low O_2 levels are part of the *in-vivo* environment for most cells). While we do not claim that data implies a specific O_2 range for "optimal" cell function, it does, combined with existing theory, suggest a more "*in-vivo-like*" set of parameters than those used in conventional cell culture. While it is likely that other processes may be affected by this change in cell BMR (e.g. drug metabolism) that is precisely the point, as these changes are likely to *more* accurately reflect cell behavior in the body. Therefore, in contrast with suggested strategies to create a suitable oxygen-rich

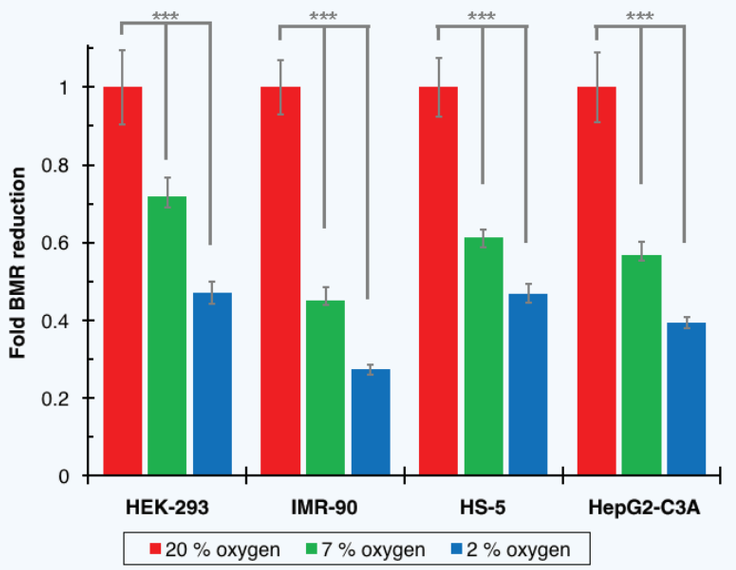

Figure 2 AlamarBlue metabolic indicator was used to measure cellular BMR in different oxygen tension environments. Correcting for the effect of oxygen on AlamarBlue fluorescence, we observed a marked decrease in respiration with falling oxygen levels across four different cell lines. A 10-fold reduction in oxygen reduced cellular respiration by a factor of nearly five. Data plotted as average ± standard deviation for $n = 7$. *** indicates $p < 0.001$ by one-way ANOVA with Tukey post-test.

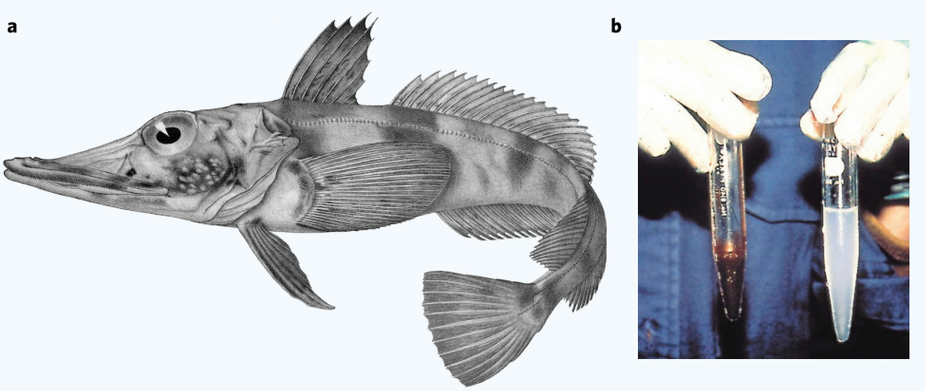

Figure 3 (**a**) Artist's rendering of *C. aceratus*, a hemoglobin-free fish living in the Southern Ocean near Antarctica. Used with permission of Regan[39]. (**b**) Freshly drawn blood from *C. aceratus* (right) is milky white while blood from Hb+ *N. coriiceps* is a familiar shade of red (left). Adapted with permission from Sidell & O'Brien[42].

blood substitute for use in an HOC[22,23,37], we propose limiting oxygen availability to manipulate cellular BMR[24]. Combined with other O_2 sensing and control systems[32–34], we may achieve normoxic or (where necessary) hypoxic conditions *in situ* to ensure that both cell- and system-level metabolic rates are appropriately scaled to those of a full-size human.

3. AN EXAMPLE OF EXTRA-PHYSIOLOGIC SURVIVAL: THE ICEFISH

The design modifications proposed in the previous section beg the question of whether such extreme departures from expected physiologic parameter values are acceptable. Would an organism with drastically altered blood O_2 carrying capacity or completely lacking hemoglobin be viable at all? Fortunately, Nature herself has provided a unique example of such extra-physiologic adaptation and survival. The family *Channichthyidae* (sometimes called 'icefish') comprises hemoglobin-negative (Hb-) fish living in the Antarctic waters of the Southern Ocean. First documented in the 1840s, initial attempts to examine the fish were thwarted by an uncooperative cat who absconded with the specimen before it could be further studied[38]. Subsequent investigations highlighted family members', including *Chaenocephalus aceratus*' (**Fig. 3a**), startling lack of blood pigment and hemoglobin (**Fig. 3b**)[39–42]. Just as technical and fundamental limitations force HOC designers to contort system parameters in strange or unexpected ways, so too has nature forced *C. aceratus* to counter its own maladaptation in order to survive.

To demonstrate, and perhaps learn from, this extra-physiologic survival, we examine the fish in more detail. As a control, we use a cousin of *C. aceratus*, *Notothenia coriiceps* (also called *neglecta*), from the common suborder *Notothenioidei*[43]. *N. coriiceps* shares a similar environment and metabolic rate (measured by oxygen consumption) as *C. aceratus*[44–46], but unlike the icefish, produces Hb at normal levels. Starting from a healthy *N. coriiceps*, we remove Hb and then apply the adaptations that allow *C. aceratus* to thrive: increasing cardiac output by a factor of nearly two and allowing for increased cutaneous respiration[40,41,44–48]. The result is a test-fish with several surprising extra-physiologic features, but nevertheless capable of survival (**Supplementary Table 1**). In particular, the ability of *C. aceratus* to absorb oxygen through its skin evokes polydimethylsiloxane (PDMS) — a common polymer in microfluidic and biomedical research applications that has similar properties of gas permeability (**Supplementary Information S1.2**).

In addition to larger-than-expected cardiac output, *C. aceratus* also has a blood volume of ~90 mL/kg, nearly twofold greater than the ~50 mL/kg expected for a fish its size[42,46,49–51]. Another member of *Channichthyidae*, *C. hamatus*, has a blood volume over twofold its predicted value[49]. These Hb- fish substantially exceed expected blood volumes yet thrive (**Supplementary Information S1.3**), reinforcing the idea that extra-normal physiology can be an acceptable mechanism to survive in the face of limitations. Related to that increased blood volume, *C. aceratus* also exhibits increased capillary density. Recent results demonstrated that three different metrics of vascularization were all ~twofold greater in *C. aceratus* than in *N. coriiceps* (**Figs. 4a and 4b**)[52]. Therefore, even though blood flow rates are double in *C. aceratus*, so too is organ blood volume, indicating that tissue residence times — a key parameter in PB-PKPD models — should also remain unchanged between it and *N. coriiceps*.

This increased vascularity also helps compensate for dilution of soluble factors (e.g. O_2, drugs or hormones) due to increased blood volume.

Table 1 Physiological values for a hypothetical 1 kg test-fish as hemoglobin (Hb) is removed and icefish characteristics introduced.

Condition imposed on the test-fish	O_2 solubility in blood [mg/mL]*	Cardiac output (Q) [mL/h]	Cutaneous respiration [mg O_2/h]	Maximum O_2 delivery [mg/h]
Normal	0.085[40]	3,900[64]	—	330
–Hb	0.0095[40]	3,900[64]	—	37
–Hb, ↑Q	0.0095[40]	7,140[48]	—	68
–Hb, ↑Q, +C. Resp.	0.0095[40]	7,140[48]	10^{41}	78
		N. coriiceps resting VO_2 = 42 mg O_2/h[45,46]		
		C. aceratus resting VO_2 = 32 mg O_2/h[44–46]		

*Measured at 0°C and 101.3 kPa.

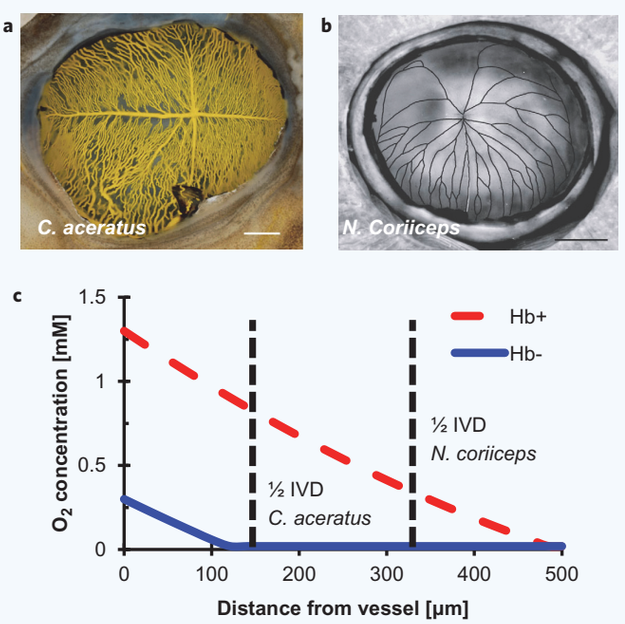

Figure 4 O_2 delivery in *Notothenioidei*. Retinal micrographs of (**a**) *C. aceratus* and (**b**) *N. coriiceps* demonstrate the difference in capillary density and intervessel distance (IVD) between the two fish. Reprinted with permission from Wujcik *et al.*[52]. (**c**) These decreased intervessel distances help compensate for low blood O_2 levels in *C. aceratus*. A similar effect should act on other solute (e.g. growth factors or drugs) diluted by larger blood volumes as well. Equation (1) solved numerically using MatLab and data from Refs. 17, 40, 52 and 53; the full list of parameter values can be found in **Supplementary Information S1.4**.

At steady state the perfusion-limited diffusion of molecules from blood into tissue is described by Equation (1):

$$D \cdot \nabla^2 C = R, \tag{1}$$

where C is the concentration, D is the diffusion coefficient and R is the uptake of solute by cells, governed in this case by Michaelis–Menten kinetics[17,53]. Although a decrease in blood concentration leads to a decrease in potential gradient to drive diffusion, a corresponding decrease in intervessel distance (IVD) suggests that solute penetration may be similar, shown here specifically for O_2 (**Fig. 4c**; parameter values in **Supplementary Information S1.4**). This icefish adaptation is another example of nature finding a holistic, multi-faceted solution to physiologically challenging conditions. Of course, applying designs such as these to an HOC may still introduce problems with drugs or molecules that act in a concentration-dependent manner on the blood vessels themselves as well as other unforeseen consequences. Conversely, these data also suggest that depletion of soluble factors (e.g. oxygen) could be achieved over shorter distances, an important design consideration for engineering organ compartments such as the liver[17,54]. Nevertheless, this preliminary analysis demonstrates that blood O_2 carrying capacity and the presence of Hb may be tuned to counter maladaptations — or possibly induce more appropriate cellular metabolic behavior. The icefish further suggests that increased blood volumes may be accommodated without drastically altering organism pharmacokinetics or certain stromal solute concentration gradients.

4. A DISTRIBUTION-INFORMED APPROACH TO HOC BLOOD VOLUME

Designing an HOC according to QPSRs alone would result in a system blood volume of ~6 µL, too small for even cutting-edge microfluidics and an acknowledged problem in the field[7,18,21,22,24]. Although a 10× (or greater) increase would yield an HOC with a more manageable circulating volume, it would also dilute soluble factors and strain physiology to a much greater extent than the ~twofold increase in volume observed in *C. aceratus*. Therefore, we adopt a pharmacokinetic approach to investigate whether and to what extent the blood volume of an HOC can be increased while maintaining physiological relevance.

When a drug is administered, only a portion circulates dissolved in the blood. Accordingly, pharmacologists define volume of distribution, V_D, to describe how much drug is available in the plasma compared to the initial dose[55,56]. Conceptually, V_D closely resembles a partition coefficient describing the equilibrium distribution of a drug between the body and the blood. Using a slightly different approach, we consider the distribution of a drug between body water — including blood — and tissue. Therefore, this treatment is most applicable to small, perfusion-limited drugs without substantial serum protein binding. This ratio, K, is defined by Equation (2):

$$K = \frac{C_T}{C_W}, \tag{2}$$

where K is the partition or distribution coefficient, C_T is the concentration of drug in body tissue and C_W is the concentration of drug in body water. Ignoring excretion and metabolism and devolving the concentration terms to amount over volume,

$$K = \frac{(Dose - X_W)/V_T}{X_W/V_W}, \tag{3}$$

where $Dose$ is the total amount of drug in the system, X_W is the amount of drug in the body water, V_T is the tissue volume and V_W is the volume of body water. Assuming no difference in concentration of drug in body water and concentration of drug in blood (C_B) and introducing V_O for non-blood body water volume (i.e. $V_W = V_B + V_O$), we rearrange to obtain Equation (5):

$$K + \frac{X_W * V_W}{V_T * X_W} = \frac{Dose}{V_T * C_B}, \quad \text{and} \tag{4}$$

$$C_B = \frac{Dose}{(V_O + V_B) + K * V_T}. \tag{5}$$

If we apply an arbitrary Z-fold increase to the blood volume compartment and normalize the result to the $Z = 1$ condition, C_{B0}, Equation (6) follows:

$$\frac{C_B}{C_{B0}} = \frac{(V_o + V_B) + K * V_T}{(V_o + Z * V_B) + K * V_T}. \quad (6)$$

In general, C_B falls as $1/Z$. However, the partitioning properties of the drug and the fact that V_B is a small fraction of the total system water volume serve to substantially temper the effect of increasing Z on blood concentration (**Supplementary Information S2**). For example, this treatment suggests that a highly hydrophilic drug, epinephrine, can tolerate ~10× increase in blood volume with only a ~twofold change in blood concentration. More hydrophobic drugs, such as amiodarone, are predicted to show almost no change in blood level at higher values of Z, and would require ~10^6 increase in blood volume to approach that same two-fold dilution.

To test these predictions, we construct a simple model of the body mimicking the two-compartment structure of our theoretical treatment. The water compartment, including variable blood volume, is represented by phosphate buffered saline and tissue is represented by an organic liquid (here, 1-octanol). The concentration of three small-molecule drugs — epinephrine, propranolol and amiodarone — was measured and normalized to the $Z = 1$ condition. The data (mean ± S.D.), along with curves representing the values predicted by Equation (6) are plotted in **Fig. 5a**. All three cases show reasonable agreement between predicted and experimental values. For scenarios where even these small dilutions are unacceptable, or in instances where the preceding treatment does not apply, other pharmacokinetic-based approaches may be useful, especially if PDMS or another gas-permeable material is used to decouple O_2 delivery from blood flow rate (**Supplementary Information S3**).

To illustrate this concept another way, we hold the aqueous phase constant, vary the mass presence of an organic depot (here represented by adipose spheroids instead of octanol) and assay for health of a HepG2 liver cell monolayer in the presence of differing concentrations of hydrophobic (amiodarone; V_D = 4,260 L for a 70-kg man) and hydrophilic (acetaminophen; V_D = 66.5 L) drugs. According to Equation (6), the high value of P for a hydrophobic compound amplifies the effects of increasing organic phase mass, leading to substantial protection of the HepG2 monolayer even at >10× the lethal concentration of amiodarone; the same changes in the face of increasing acetaminophen dosing shows no such effect (**Fig. 5b**). Combined with the theoretical treatment developed here for solutes of varying hydrophobicity in aqueous and organic phases of varying volume, these results demonstrate that HOC designers may be able to systematically predict the effects of changing system fluid volumes and therefore compensate for such changes in their experimental design.

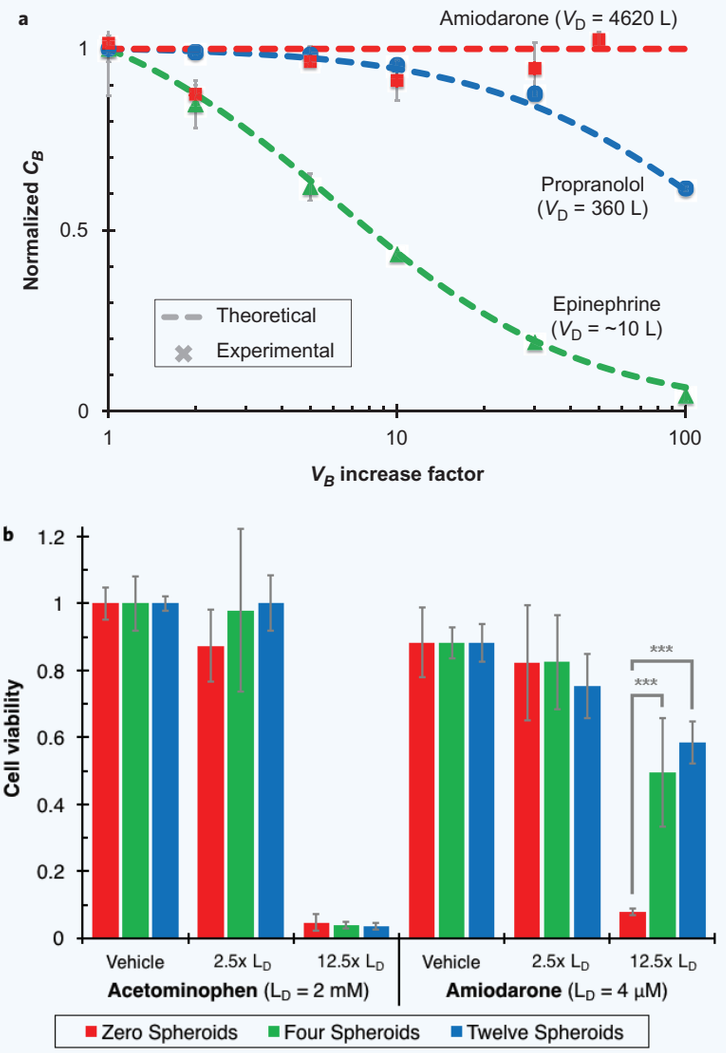

Figure 5 Altering aqueous to organic volume proportions affects concentration and toxicity of various drugs. (**a**) Increased blood volumes minimally effect blood concentration depending on drug properties for perfusion-limited drugs according to Equation (6). Hydrophobic drugs (e.g. amiodarone) partition mostly to tissue and blood concentration is largely unaffected by changes in blood volume. More hydrophilic drugs (e.g. epinephrine) partition largely to the blood and are more affected by large changes in blood volume. (**b**) In a live-cell experiment, increasing mass of the organic phase (i.e. addition of more adipospheroids) rescues HepG2-C3A liver cells from toxicity of a hydrophobic drug (Amiodarone, lethal dose 4 μM), but not a hydrophilic drug (acetaminophen, lethal dose 2 mM). Data plotted as average ± S.D. for $n = 7$.

*** indicates $p < 0.001$ by two-way ANOVA with Tukey post-test.

5. HOC DESIGN

5.1 Organ compartment design strategy

To design each organ compartment, we build on metabolically supported functional scaling (MSFS) strategies proposed previously, as well as other, similar, schemes[22,24,57]. The specific approach of Moraes *et al.* classifies organs according to principle function: two-dimensional (F-2D) or membranous tissue (e.g. lung) is scaled by surface area while functionally three-dimensional (F-3D) or lobular tissue (e.g. adipose) is scaled by volume[24]. Since this approach relies on principles of Euclidian geometry, it avoids inconsistencies that appear when empirical laws are extrapolated outside the range of the original dataset — a key problem for applying empirical, allometric organ–organism size relationships to HOC design[22,23]. Design parameters for F-2D organs are achieved by scaling according to surface area and compartment size is selected to match fluidic shear values found *in vivo* for each tissue. F-3D organs are simply scaled by mass. For more complicated organs that may be classified as both F-2D and F-3D (e.g. liver), we used a two-compartment approach: one section with high surface area and another with high mass

Table 2 Design strategy for different HOC organ compartment classes defined by metabolically supported functional scaling (MSFS) theory.

HOC organ compartment class	Tissue size	Blood volume
F-2D	Surface area constrained, μM^1 scaling from macro human	Dimensions selected to maintain physiologic shear given fractional cardiac output
F-3D	Volume constrained, μM^1 scaling from macro human	Calculated so that organ blood volume matches target fractional organ mass of whole body
F-2.5D	Divided into F-2D and F-3D domains with each domain scaled per F-2D or F-3D design rules	

that together approach the appropriate values (**Table 2**). Spheroids and other tissue aggregation strategies may be particularly useful in these cases (**Supplementary Information S4**).

The endothelium presents another special case. Since several sources estimate the endothelial surface area of the body at 1,000 m^2 or greater[58–60], including the whole of the endothelium in this HOC would be an impossible undertaking. Since the endothelium mainly acts in concert with its associated organ rather than as a distinct entity, we include only endothelial tissue from organs already represented in this model (lung and liver). These tissues serve to recapitulate endothelial cell function within the organs included in this design and also provide a readout for general endothelial "health" across the HOC.

In addition to the organs *explicitly* included in this HOC design, we must also account for the body volume not represented by any of the designated organ compartments. Including a blank "other organs" zone to represent *implied* (but absent) organs ensures that our total system mass will be commensurate with that of a macro version and other groups have included "missing organ formulators" and "other tissues" compartments to similar ends[19,20,22,24]. Importantly, since we justify a substantially increased blood volume based in part on a volume distribution-based treatment that considers the entire body volume, it is critical that volume be faithfully replicated in our model system.

2. Lack of Hb or an Hb substitute does not doom a vertebrate organism (or an HOC) *ex ante*. In fact, by introducing systemic redundancies and extra-normal physiologic values nature has, and engineers may, successfully addressed such anomalies.
3. Blood volume increases are necessary to address technical limitations of current tissue engineering and microfabrication techniques. A distribution-based treatment of supra-physiologic blood volumes and the example of the icefish indicate that designers have some latitude in determining HOC blood volume, especially for perfusion-limited drugs.

It is necessary to note here that increasing blood volume is not at odds with our proposal to limit oxygen supply. Since Henry's law dictates that the concentration of gas dissolved in a liquid is proportional to the partial pressure of that gas in the atmosphere and (as **Fig. 2** demonstrates) cell consume oxygen in a concentration dependent manner, the overall blood volume should have little bearing on the matter in an oxygen controlled environment. If, rather than controlling the pO_2 of the culture atmosphere, a researcher sought to generate low O_2 by balancing gas exchange, consumption and flow[61], then changing blood volume may indeed necessitate a careful balance of various parameters (e.g. flow, volume, cellular O_2 consumption and media oxygen concentration).

Finally, we formalize a complete set of design parameters for a lung, liver, endothelium, fat, and heart $\times 10^{-6}$ HOC (**Table 3**, other tables and comparisons in **Supplementary Information S5**) that follows the design principles laid out here. We further compare relevant design criteria of this more practical $\times 10^{-6}$ HOC to *C. aceratus*, a standard human, and a mouse (**Fig. 6a**). Values for this five-parameter comparison across blood oxygen content (blood O_2), intervessel distance (IVD), skin gas exchange, cardiac output and blood volume were drawn from many sources and normalized against values predicted by QPSRs[17,23,40,46,48,49,51,52,62-72]. For details, see **Supplementary Information S6**. Another set of charts predicting behavior based on these parameters is calculated and shown

5.2 Overall design parameters

The insights provided by our examinations of metabolic scaling, *C. aceratus*' unique physiology, and volume of distribution considerations indicate that we need not be confined by preconceived notions of what is or is not "physiologic" in designing an HOC. Instead, it is the ultimate response — the function — of the HOC and not the underlying structure that is paramount. Specifically:

1. Without additional controls, on-chip cellular BMR will exceed *in-vivo* levels and cause a fundamental mismatch between the model system and reality. We propose limiting oxygen delivery as one effective mechanism for controlling cellular BMR.

Table 3 A comprehensive table of design parameters for a five-organ $\times 10^{-6}$ HOC. We propose increasing blood volume levels beyond those called for by conventional quarter-power scaling relationships (QPSRs) to account for engineering limitations in organ design. Chamber dimensions are selected to match *in-vivo* shear levels (F-2D) or match *in-vivo* mass (F-3D).

Organ		Class	$\times 10^{-6}$ HOC							
			Surface area [mm^2]	Tissue mass [mg]	Blood volume (BV) [µL]	% BV	% CO	Compartment dimension		
								Length [mm]	Width [mm]	Height [mm]
Lung	*Endothelium*	*F-2D*	*30*	*0.12*	*1.1*	—	—	—	—	—
	Non-EC	*F-2D*	*40*	*0.16*	*1.4*	—	—	—	—	—
	Total	F-2D	70	0.28	2.5	4	100	9.02	7.76	0.035
Liver	*Endothelium*	*F-2D*	*80*	*0.32*	*2*	—	—	14.87	5.38	0.025
	Non-EC	*F-3D*	*34*	*1.75*	*1.03*	—	—	1.57	1.57	1
	Total	F-2/3D	114	2.07	3.03	5	25	—	—	—
Heart		F-3D	—	0.33	0.28	0.5	4	1.06	1.06	0.5
Fat		F-3D	—	12.5	10.7	18	5	4.96	4.96	1
Blood		—	—	—	60	—	—	—	—	—
"Other Tissues"		F-3D	—	48.8	43.5	73	66	6.6	6.6	1
Blood Oxygen Content [BL_{O2}; mM]						~2				
Cutaneous Respiration [mol/m/s/mmHg]						$\leq 3.8 \times 10^{-11}$				
Cardiac Output [mL/s]						3.4×10^{-3}				
Intervessel Distance [IVD; µm]						250				

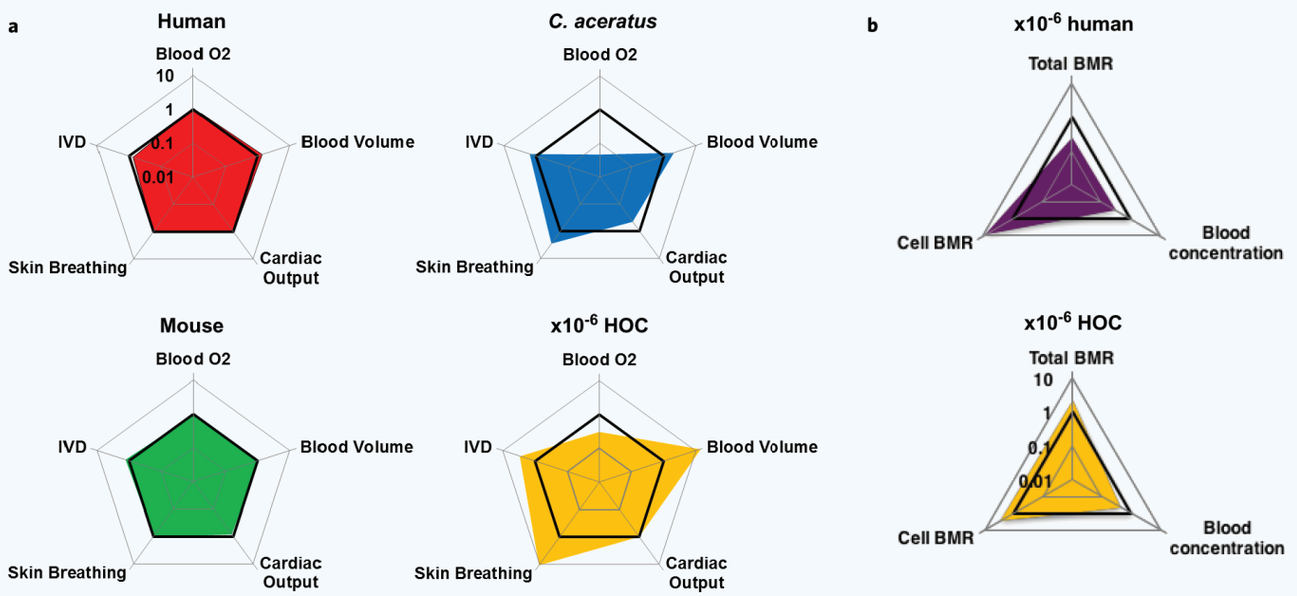

Figure 6 Design and performance of natural and artificial physiological systems. (**a**) Radar charts comparing *design* parameter values for a human, a mouse, the Hb– icefish *C. Aceratus*, and a $\times 10^{-6}$ miniaturized HOC. Values plotted on a log scale and normalized to QPSR estimates for all graphs. Note that observed values for the mouse and human match QPSR estimates (bold lines) closely while the general shape of the charts for *C. Aceratus* and the HOC have similar shapes. A $\times 10^{-6}$ human designed only according to QPSRs would lie exactly along the bolded line representing a normalized value of 1. Without additional controls, this $\times 10^{-6}$ model would have abnormally high per cell and system metabolism. (**b**) Applying the modifications proposed here to build a $\times 10^{-6}$ HOC is predicted to lead to a more accurate model of the human body measured across three key *functional* parameters. Compared to an QPSR-scaled $\times 10^{-6}$ human with a minimum blood volume limited by technical challenges (top) and despite straying from conventional parameters, our design strategy yields a $\times 10^{-6}$ HOC (bottom) that more closely matches human levels of cellular BMR, system BMR and blood concentration of a low volume distribution drug (e.g. epinephrine). Computed using data from Refs. 17, 23, 40, 46, 48, 49, 51, 52, 62–72.

in (**Fig. 6b**), demonstrating the superiority of our holistic design strategy over an unmodified approach.

Inspired by the example of *C. aceratus* and motivated to suppress cellular BMR to physiologic levels (and to avoid the challenges inherent in developing a synthetic substitute), we have deliberately excluded Hb from this HOC design in order to restrict oxygen availability and limit cellular BMR. However, Hb also plays a key role in transporting carbon dioxide away from metabolically active tissues — carrying up to 30% of the CO_2 transported in blood[70]. In this HOC design, we justify ignoring these effects because CO_2 transport can occur by other means. At 35°C, PDMS is nearly five times more permeable to carbon dioxide than oxygen[73]. Similarly, the solubility of CO_2 and NO (nitrous oxide, an important signaling molecule) in water are both orders of magnitude greater than O_2[74–76]. Beyond oxygen transport, Hb plays important roles in other aspects of physiology including NO catalysis[70]. Depending on the specific application, each function may need to be explicitly accounted for in HOC design.

For this (or any) HOC system to be accepted as a microphysiological model of the body, some method of validating the underlying design strategy is necessary. Although directly testing such a system against humans may be challenging, we can apply the same design criteria outlined here to build rats-, mice-, etc.-on-a-chip. Parallel studies comparing the response of the microphysiological model system to the genuine animal will provide information on areas where HOCs may be particularly well- (or ill-)suited to serve as a complimentary research tool. A second approach may be to test whether an HOC is able to maintain key homeostatic parameters (e.g. blood glucose level) in the face of a reasonable challenge (e.g. bolus injection of glucose). In and of themselves, these experiments may also yield new mechanistic insights into previously unexplored aspects of common biomedical research models.

6. CONCLUSION

This work makes several key assumptions that should be verified, or at least noted, in further research. Although the section on 'Control of Cellular BMR' makes clear that we may indeed induce a more *in-vivo*-like BMR in cells by controlling the concentration of oxygen available in culture, this is not the only criterion necessary for success. Many other factors including ECM support and cell–cell interaction, and likely some yet to be discovered factors, also drive *in-vivo*-like phenotypes and must be carefully considered as part of any HOC effort. Furthermore, for the treatment of the proposed distribution-informed approach to HOC blood volume to be valid, experimentalists must know, or at least be able to suspect, the chemical properties of all drugs, metabolites and other molecules of interest within a system. To be exhaustive within a generalized experimental model, it may be necessary for researchers to use iterative processes, where a system is screened for compounds of interest then tuned accordingly and rescreened. Finally, the F-2D and F-3D classification proposed for HOC designs is likely too simplistic. While some organs fall readily into one category or the other, the truth is that most all organs behave somewhat like the liver — each has critical dependencies on *both* surface area and volume. To most accurately represent this reality, engineered, organ-specific on-chip systems would ideally represent organ compartment. However, in many cases constraints on resources and/or complexity will mean that F-2D and F-3D idealizations are sufficient in most instances.

Quarter power scaling relationships are both empirically and theoretically supported and provide guidance for sizing physiologic parameters in the face of changing system size. Their application to the development of microphysiological models of the body or "HOCs" however introduces both fundamental and technical challenges which currently frustrate efforts at design and construction of a relevant, feasible system. We posit that HOC designers may avoid these issues by selecting parameters outside the realm of what is considered physiologic so long as the ultimate function of the system is preserved. Since cell behavior is context dependent, suppressing cellular BMR on-chip to mimic *in-vivo* levels is crucial to designing a physiologically relevant HOC. We observe O_2-dependent decreases in cell metabolism across four different cell types to demonstrate the feasibility of this approach. We use a natural experiment, the icefish, to conceptually justify this approach and demonstrate how extra-physiologic parameters may interact to give a normal physiologic response. Further study of an HOC system through a distribution-informed treatment of blood concentration of small-molecule drugs indicates that we may indeed increase HOC blood volumes with only minor consequences. In cases where even that is unacceptable, we provide frameworks to estimate the magnitude of and/or mitigate the error. Integrating these lessons in the design of a liver–lung–heart–fat–blood system, we propose a complete set of design parameters for a $\times 10^{-6}$ miniaturized HOC system. This work forms a basis of a nature-inspired approach to govern the design of *in-vitro* model systems.

7. METHODS

7.1 Oxygen conformance and cellular BMR suppression

All cell lines were obtained from ATCC and cultured in Dulbecco's Modified Eagle Medium (DMEM) supplemented with 10% Fetal Bovine Serum (FBS) and 1% antibiotic/antimycotic (anti/anti). The day before the experiment, cells were seeded in 96-well plates at 25,000 cells/well and allowed to adhere overnight. OxyCycler atmosphere control chambers (BioSphyrix, New York) were set to 2% and 7% oxygen, both with 5% CO_2. The day of the experiment, media was changed to DMEM and anti/anti without FBS and one plate was placed in each oxycycler chamber, as well as a third plate in a standard cell culture incubator (20% O_2 and 5% CO_2) and allowed to equilibrate for four hours. At that point, the media was changed again and replaced with DMEM, anti/anti and AlamarBlue metabolic indicator (Invitrogen). After a two-hour incubation, the level of reduced AlamarBlue was measured using a fluorescent plate reader (BioTek Synergy Neo) at 560/590 nm (excitation/emission).

AlamarBlue indicates cell metabolic activity by serving as an oxidizing agent during aerobic respiration, competing with oxygen for electrons at the end of the electron transport chain[70,77]. Changing oxygen levels, therefore, affect the frequency at which AlamarBlue is reduced and therefore the levels of fluorescence observed across each cell culture plate at the end of the experiment. To correct for this effect, we use Equation (7) to estimate cellular metabolic activity in the face of changing oxygen level:

$$Cellular\ BMR = AB_{Red} * \frac{\Delta P_{AB} + X * \Delta P_{O2}}{\Delta P_{AB}}, \quad (7)$$

where *Cellular BMR* is the corrected, unitless cellular metabolic rate measured by AlamarBlue, AB_{Red} is the fluorescent measurement from the assay, ΔP_{AB} is the difference in reduction potential between AlamarBlue and cytochrome C, the ultimate reducing agent of oxygen in aerobic respiration, X is the fractional reduction of oxygen tension compared to a 20% O_2 atmosphere (typical for a laboratory cell culture incubator) and ΔP_{O2} is the difference in reduction potential between O_2 and cytochrome C. Using standard values to calculate ΔP[77], we can generate a corrected cellular BMR. We may use this unitless metric to compare relative cellular BMRs and to demonstrate the effect of oxygen tension on cellular metabolic activity. Two caveats must apply to this analysis, however. First, the cellular BMR values compared here are *aerobic* only; we make no effort to measure energy derived from fermentation. As respiration is an order of magnitude more efficient, any error introduced by this approach is likely to be sufficiently small. Second, while these cellular BMRs are purely *relative* measurements, one may theoretically use a series of calibration experiments to arrive at a set of *absolute* measurements for cellular metabolic rates.

7.2 Distribution-informed approach to HOC blood volumes

To test the theoretical predictions of Equation (6) regarding the behavior of small-molecule drugs in the face of changing blood volumes, we constructed a crude, $\times 10^{-5}$ "pharmacokinetics-in-a-tube" system. A glass vial containing 280 µL of 1-octanol (Sigma) was used to model the tissue volume of a $\times 10^{-5}$ human and 360 µL of pH 7.4 phosphate-buffered saline (PBS, Life Technologies) represented the non-blood body water volume[55,56]. A variable amount of PBS was used to represent $Z = 1$, 2, 5, 10, 30, 50 and 100 conditions, where $Z = 1$ corresponded to a blood volume of 60 µL. The relevant drug was added to the vial, agitated, and allowed to equilibrate for ~two hours in a 5% CO_2 incubator at 37°C. After ~two hours, the organic and aqueous phases were well separated and the appropriate phase was sampled and analyzed. Each condition was performed in triplicate. For epinephrine (Sigma), a total dose of 100 µg/vial was used and the lower (aqueous) phase was sampled. Epinephrine levels were detected by an Acquity UPLC system (Waters) with a reverse-phase C18 column (Waters) and a UV-vis detector measuring absorbance at 210 nm. The mobile phase was 99% 20 mM NaH_2PO_4 at pH 2.5 and 1% MeOH. For propranolol, a total dose of 1 mg/vial was used and the aqueous phase was sampled. Propranolol (Sigma) levels were detected on a Synergy plate reader (BioTek) by reading fluorescence at 289/353 nm. For amiodarone (Sigma), the total dose/vial was 0.56 mg and the upper (organic) phase was sampled. Amiodarone levels were detected by fluorescence at 388/475 nm.

To investigate the implications of changing organic phase mass on a living system, we used a liver-adipospheroid co-culture platform. 3T3-L1 preadipocytes were expanded and differentiated into adipose tissues in 3D spheroid culture as described previously with 8,000 cells per spheroid[24]. HepG2-C3A liver cells were seeded in a clear bottom, black-wall 96-well plate (Corning Costar) at a density of 10,000 cells/well and given six hours to attach. After adipose spheroid differentiation, the spheroids were collected from the hanging drop plate and added to the 2D liver cell culture (0, 4 or 12 per well) in 30 µL of media volume. Amiodarone (dissolved in DMSO) and acetaminophen were then added to the culture wells and incubated for 24 hours. After the incubation period, media and spheroids were aspirated and the HepG2-C3A monolayer was washed once gently and AlamarBlue indicator was added. HepG2 viability was measured by taking a fluorescence reading at 560/590 (ex/em) after two hours. Data was analyzed using two-way ANOVA with Tukey's post-test.

ACKNOWLEDGEMENTS

The authors are indebted to Prof. Duxin Sun for helpful discussion regarding drug distribution and pharmacokinetics and Rose Ackerman and Prof. Steve Schwendeman for assistance with UPLC.

The authors gratefully acknowledge funding by the Defense Threat Reduction Agency (DTRA) under Space and Naval Warfare Systems Center Pacific (SSC PACIFIC) Contract No. N66001-13-C-2027. The content is solely the responsibility of the authors and does not necessarily represent the official views of the awarding agency. JML gratefully acknowledges support from the University of Michigan Tissue Engineering and Regenerative Medicine Training Program (NIH T32-DE007057), a U.S. Department of Education GAANN fellowship, and the University

of Michigan Microfluidics in Biomedical Sciences Training Program (NIH T32 EB005582-05). CM gratefully acknowledges support from the Natural Sciences and Engineering Research Council of Canada and the Banting postdoctoral fellowship program.

REFERENCES

1. Huh, D. *et al*. Reconstituting organ-level lung functions on a chip. *Science* **328**(5986), 1662–1668 (2010).
2. Moraes, C., Mehta, G., Lesher-Perez, S.C. & Takayama, S. Organs-on-a-chip: A focus on compartmentalized microdevices. *Ann. Biomed. Eng.* **40**(6), 1211–1227 (2012).
3. Bhatia, S.N. & Ingber, D.E. Microfluidic organs-on-chips. *Nat. Biotechnol.* **32**(8), 760–772 (2014).
4. Sung, J.H. *et al*. Microfabricated mammalian organ systems and their integration into models of whole animals and humans. *Lab Chip* **13**(7), 1201 (2013).
5. Sung, J.H., Kam, C. & Shuler, M.L. A microfluidic device for a pharmacokinetic–pharmacodynamic (PK–PD) model on a chip. *Lab Chip* **10**(4), 446 (2010).
6. Vozzi, F., Heinrich, J.-M., Bader, A. & Ahluwalia, A.D. Connected culture of murine hepatocytes and human umbilical vein endothelial cells in a multicompartmental bioreactor. *Tissue Eng. Part A* **15**(6), 1291–1299 (2008).
7. Maschmeyer, I. *et al*. A four-organ-chip for interconnected long-term co-culture of human intestine, liver, skin and kidney equivalents. *Lab Chip* **15**(12), 2688–2699 (2015).
8. Esch, M.B. *et al*. How multi-organ microdevices can help foster drug development. *Adv. Drug Deliv. Rev.* **69–70**, 158–169 (2014).
9. National Center for Advancing Translational Sciences (NCATS). Tissue chip for drug screening (2012), ncats.nih.gov/tissue-chip.html
10. Polini, A. *et al*. Organs-on-a-chip: A new tool for drug discovery. *Expert Opin. Drug Discov.* **9**(4), 335–352 (2014).
11. Kleiber, M. Body size and metabolic rate. *Physiol. Rev.* **27**(4), 511–541 (1947).
12. White, C.R. Allometric scaling of mammalian metabolism. *J. Exp. Biol.* **208**(9), 1611–1619 (2005).
13. West, G.B., Brown, J.H. & Enquist, B.J. A general model for the origin of allometric scaling laws in biology. *Science* **276**(5309), 122–126 (1997).
14. Banavar, J.R. *et al*. A general basis for quarter-power scaling in animals. *Proc. Natl. Acad. Sci. USA* **107**(36), 15816–15820 (2010).
15. Iori, E. *et al*. Glucose and fatty acid metabolism in a 3 tissue *in-vitro* model challenged with normo- and hyperglycaemia. *PLoS ONE* **7**(4), e34704 (2012).
16. Mazzei, D., Guzzardi, M.A., Giusti, S. & Ahluwalia, A. A low shear stress modular bioreactor for connected cell culture under high flow rates. *Biotechnol. Bioeng.* **106**(1), 127–137 (2010).
17. Mattei, G., Giusti, S. & Ahluwalia, A. Design criteria for generating physiologically relevant *in vitro* models in bioreactors. *Processes* **2**(3), 548–569 (2014).
18. Marx, U. *et al*. "Human-on-a-chip" developments: A translational cutting-edge alternative to systemic safety assessment and efficiency evaluation of substances in laboratory animals and man? *Altern. Lab Anim.-ATLA* **40**(5), 235 (2012).
19. Viravaidya, K., Sin, A. & Shuler, M.L. Development of a microscale cell culture analog to probe naphthalene toxicity. *Biotechnol. Prog.* **20**(1), 316–323 (2004).
20. Esch, M.B., Mahler, G.J., Stokol, T. & Shuler, M.L. Body-on-a-chip simulation with gastrointestinal tract and liver tissues suggests that ingested nanoparticles have the potential to cause liver injury. *Lab Chip* **14**(16), 3081 (2014).
21. Abaci, H.E. & Shuler, M. Human-on-a-chip design strategies and principles for physiologically based pharmocokinetics/pharmacodynamics modeling. *Integr. Biol.* **7**(4), 383–391 (2015).
22. Wikswo, J.P. *et al*. Engineering challenges for instrumenting and controlling integrated organ-on-chip systems. *IEEE Trans. Biomed. Eng.* **60**(3), 682–690 (2013).
23. Wikswo, J.P. *et al*. Scaling and systems biology for integrating multiple organs-on-a-chip. *Lab Chip* **13**(18), 3496 (2013).
24. Moraes, C. *et al*. On being the right size: Scaling effects in designing a human-on-a-chip. *Integr. Biol.* **5**(9), 1149 (2013).
25. West, G.B., Woodruff, W.H. & Brown, J.H. Allometric scaling of metabolic rate from molecules and mitochondria to cells and mammals. *Proc. Natl. Acad. Sci. U. S. A.* **99**(Suppl. 1), 2473–2478 (2002).
26. Porter, R.K. & Brand, M.D. Cellular oxygen consumption depends on body mass. *Am. J. Physiol.-Regul. Integr. Comp. Physiol.* **269**(1), R226–R228 (1995).
27. Brown, M.F., Gratton, T.P. & Stuart, J.A. Metabolic rate does not scale with body mass in cultured mammalian cells. *Am. J. Physiol. Regul. Integr. Comp. Physiol.* **292**(6), R2115–R2121 (2007).
28. Heusner, A.A. Size and power in mammals. *J. Exp. Biol.* **160**(1), 25–54 (1991).
29. Wang, W., Upshaw, L., Strong, D.M., Robertson, R.P. & Reems, J. Increased oxygen consumption rates in response to high glucose detected by a novel oxygen biosensor system in non-human primate and human islets. *J. Endocrinol.* **185**(3), 445–455 (2005).
30. Wataha, J.C., Hanks, C.T. & Craig, R.G. *In vitro* effect of metal ions on cellular metabolism and the correlation between these effects and the uptake of the ions. *J. Biomed. Mater. Res.* **28**(4), 427–433 (1994).
31. Huang, G. & Greenspan, D.S. ECM roles in the function of metabolic tissues. *Trends Endocrinol. Metab.* **23**(1), 16–22 (2012).
32. Mehta, G. *et al*. Quantitative measurement and control of oxygen levels in microfluidic poly(dimethylsiloxane) bioreactors during cell culture. *Biomed. Microdevices* **9**(2), 123–134 (2007).
33. Lo, J.F., Sinkala, E. & Eddington, D.T. Oxygen gradients for open well cellular cultures via microfluidic substrates. *Lab Chip* **10**(18), 2394 (2010).
34. Oppegard, S.C., Nam, K.-H., Carr, J.R., Skaalure, S.C. & Eddington, D.T. Modulating temporal and spatial oxygenation over adherent cellular cultures. *PLoS ONE* **4**(9), e6891 (2009).
35. Schumacker, P.T., Chandel, N. & Agusti, A.G. Oxygen conformance of cellular respiration in hepatocytes. *Am. J. Physiol. Lung Cell. Mol. Physiol.* **265**(4), L395–L402 (1993).
36. Ahluwalia, A. Allometric scaling *in-vitro*. *Sci. Rep.* **7**, 42113 (2017).
37. Wikswo, J.P. The relevance and potential roles of microphysiological systems in biology and medicine. *Exp. Biol. Med.* **239**(9), 1061–1072 (2014).
38. Gon, O. & Heemstra, P.C. *Fishes of the Southern Ocean* (J.L.B. Smith Institute of Icdhthyology, South Africa, 1990).
39. Regan, C.T. II. The Antarctic fishes of the Scottish National Antarctic expedition. *Trans. R. Soc. Edinb.* **49**(02), 229–292 (1913).
40. Ruud, J.T. Vertebrates without erythrocytes and blood pigment. *Nature* **173**(4410), 848–850 (1954).
41. Hemmingsen, E.A. Respiratory and cardiovascular adaptations in hemoglobin-free fish: Resolved and unresolved problems. In *Biology of Antarctic Fish* (ed.) di Prisco, G., Maresca, B. & Tota, B. (Springer, 1991), pp. 191–203.
42. Sidell, B.D. & O'Brien, K.M. When bad things happen to good fish: The loss of hemoglobin and myoglobin expression in Antarctic icefishes. *J. Exp. Biol.* **209**(10), 1791–1802 (2006).
43. FishBase. *Notothenia coriiceps* (2005), http://www.fishbase.se/Photos/PicturesSummary.php?ID=4702&what=species
44. Ralph, R. & Everson, I. The respiratory metabolism of some Antarctic fish. *Comp. Biochem. Physiol.* **27**, 299–307 (1968).
45. Holeton, G.F. Oxygen uptake and circulation by a hemoglobinless Antarctic fish (*Chaenocephalus aceratus* Lonnberg) compared with three red-blooded Antartic fish. *Comp. Biochem. Physiol.* **34**(2), 457–471 (1970).
46. Hemmingsen, E.A. & Douglas, E.L. Respiratory characteristics of the hemoglobin-free fish *Chaenocephalus aceratus*. *Comp. Biochem. Physiol.* **33**(4), 733–744 (1970).
47. Egginton, S. Blood rheology of Antarctic fishes: Viscosity adaptations at very low temperatures. *J. Fish Biol.* **48**(3), 513–521 (1996).
48. Hemmingsen, E.A., Douglas, E.L., Johansen, K. & Millard, R.W. Aortic blood flow and cardiac output in the hemoglobin-free fish *Chaenocephalus aceratus*. *Comp. Biochem. Physiol. A Physiol.* **43**(4), 1045–1051 (1972).
49. Acierno, R., MacDonald, J.A., Agnisola, C. & Tota, B. Blood volume in the hemoglobinless Antarctic teleost *Chionodraco hamatus* (Lönnberg). *J. Exp. Zool.* **272**(5), 407–409 (1995).
50. Eastman, J.T. *Antarctic Fish Biology: Evolution in a Unique Environment* (Academic Press Limited, 1993).
51. Twelves, E.L. Blood volumes of two Antarctic fishes. *Antarct. Surv. Bull.* **31**, 85–92 (1972).
52. Wujcik, J.M., Wang, G., Eastman, J.T. & Sidell, B.D. Morphometry of retinal vasculature in Antarctic fishes is dependent upon the level of hemoglobin in circulation. *J. Exp. Biol.* **210**(5), 815–824 (2007).
53. Bianconi, E. *et al*. An estimation of the number of cells in the human body. *Ann. Hum. Biol.* **40**(6), 463–471 (2013).
54. Allen, J.W. & Bhatia, S.N. Formation of steady-state oxygen gradients *in vitro*: Application to liver zonation. *Biotechnol. Bioeng.* **82**(3), 253–262 (2003).
55. Shargel, L. & Yu, A.B.C. *Applied Biopharmaceutics and Pharmacokinetics* (Appleton & Lange, 1993).
56. Rowland, M. & Tozer, T.N. *Clinical Pharmacokinetics: Concepts and Applications* (Williams & Wilkins, 1995).
57. Sbrana, T. & Ahluwalia, A. Engineering Quasi-Vivo® *in vitro* organ models. *Adv. Exp. Med. Biol.* **745**, 138–153 (2012).
58. Wolinsky, H. A proposal linking clearance of circulating lipoproteins to tissue metabolic activity as a basis for understanding atherogenesis. *Circ. Res.* **47**(3), 301–311 (1980).
59. Jaffe, E.A. Cell biology of endothelial cells. *Hum. Pathol.* **18**(3), 234–239 (1987).
60. Augustin, H.G., Kozian, D.H. & Johnson, R.C. Differentiation of endothelial cells: Analysis of the constitutive and activated endothelial cell phenotypes. *BioEssays* **16**(2), 901–906 (1994).
61. Mehta, G. *et al*. Hard top soft bottom microfluidic devices for cell culture and chemical analysis. *Anal. Chem.* **81**(10), 3714–3722 (2009).
62. Petschow, R., Petschow, D., Bartels, R., Baumann, R. & Bartels, H. Regulation of oxygen affinity in blood of fetal, newborn and adult mouse. *Respir. Physiol.* **35**(3), 271–282 (1978).
63. Williams, L.R. & Leggett, R.W. Reference values for resting blood flow to organs of man. *Clin. Phys. Physiol. Meas.* **10**(3), 187 (1989).
64. Egginton, S. Control of tissue blood flow at very low temperatures. *J. Therm. Biol.* **22**(6), 403–407 (1997).
65. Tournoux, F. *et al*. Validation of noninvasive measurements of cardiac output in mice using echocardiography. *J. Am. Soc. Echocardiogr.* **24**(4), 465–470 (2011).
66. Stücker, M. *et al*. The cutaneous uptake of atmospheric oxygen contributes significantly to the oxygen supply of human dermis and epidermis. *J. Physiol.* **538**(3), 985–994 (2002).

67. Brandrup, J., Immergut, E.H. & Grulke, E.A. *Polymer Handbook* (John Wiley & Sons, 1998).
68. Folarin, A.A., Konerding, M.A., Timonen, J., Nagl, S. & Pedley, R.B. Three-dimensional analysis of tumour vascular corrosion casts using stereoimaging and micro-computed tomography. *Microvasc. Res.* **80**(1), 89–98 (2010).
69. Malkusch, W., Konerding, M.A., Klapthor, B. & Bruch, J. A simple and accurate method for 3-D measurements in microcorrosion casts illustrated with tumour vascularization. *Anal. Cell. Pathol.* **9**(1), 69–81 (1995).
70. Widmaier, E.P., Raff, H. & Strang, K.T. *Vander's Human Physiology* (McGraw-Hill, 2006).
71. Peters, R.H. *The Ecological Implications of Body Size* (Cambridge University Press, 1983).
72. Schmidt-Nielsen, K. *Scaling: Why Is Animal Size So Important?* (Cambridge University Press, 1984).
73. Merkel, T.C., Bondar, V.I., Nagai, K., Freeman, B.D. & Pinnau, I. Gas sorption, diffusion, and permeation in poly (dimethylsiloxane). *J. Polym. Sci. B Polym. Phys.* **38**(3), 415–434 (2000).
74. Weiss, R.F. The solubility of nitrogen, oxygen and argon in water and seawater. *Deep Sea Res. Oceanogr. Abstr.* **17**(4), 721–735 (1970).
75. Weiss, R.F. Carbon dioxide in water and seawater: The solubility of a non-ideal gas. *Mar. Chem.* **2**, 203–215 (1974).
76. Weiss, R.F. & Price, B.A. Nitrous oxide solubility in water and seawater. *Mar. Chem.* **8**, 347–359 (1980).
77. Invitrogen. AlamarBlue Technical Datasheet, https://tools.thermofisher.com/content/sfs/manuals/PI-DAL1025-1100_TI%20alamarBlue%20Rev%201.1.pdf

SUPPLEMENTARY INFORMATION

S1. Icefish analyses

S1.1 *Detailed derivation of extra-physiologic parameter comparison between Notothenia coriiceps and Chaenocephalus aceratus*

Here, we use a natural experiment to demonstrate that the absence of hemoglobin (Hb) alone does not doom a vertebrate — or our HOC — *ex ante*. Furthermore, this extra-ordinary example — nature using two wrongs to make a right — illustrates workarounds and adaptations that may be generally useful to HOC designers.

S1.1.1 Antarctic, hemoglobin-positive (Hb+) fish deliver sufficient O_2 through blood

A thorough examination of the oxygen delivery system of an Hb-less (Hb–) animal can provide both specific and abstract clues for addressing fundamental and technical challenges of HOC design. We begin by examining *C. aceratus*' cousin, *Notothenia coriiceps* (also called *neglecta*), from the common suborder *Notothenioidei*[S1]. *N. coriiceps* is also found in the ice-cold waters surrounding Antarctica but unlike *C. aceratus,* the fish expresses Hb at normal levels. Further, literature reports indicate that *N. coriiceps* and *C. aceratus* have overlapping ranges of metabolic rate, as measured by oxygen consumption[S2–S4]. By methodically imposing some of the characteristics that make members of the family *Channicthyidae* special upon a hypothetical *N. coriiceps* test-fish from a similar environment we can learn how those adaptations may inform our own design and fabrication of a human on a chip system whose parameters will inevitably deviate from actual humans to some degree.

To examine how much oxygen is delivered by the blood for a given scenario, we multiply the cardiac output, Q (normalized for a 1 kg fish, the approximate average mass for both *C. aceratus* and *N. coriiceps*)[S2-S5], by the oxygen blood level, BL_{O2}. Since reptiles, amphibians, fish and even (in limited cases) mammals have been known to conduct gas exchange through the surface of their skin[S6], we also use published reports to account for this source of oxygen. Comparing the results to measured oxygen consumption values, VO_2, we may assess whether the circulatory system of the fish is can support its metabolism. Previous studies on *N. coriiceps* measured a resting Q of 3,900 mL blood/hour[S5]. Since this fish produces Hb, BL_{O2} is 0.06 mL O2/mL blood[S7]. Therefore, the circulatory system of the fish can deliver 230 mL O_2/hour or, at 0°C and atmospheric pressure, 330 mg O_2/hour. Since the cutaneous respiration of larger, scaled fish is generally small[S8], we omit any "skin breathing" adjustment for *N. coriiceps*. At rest, the average VO_2 of *N. coriiceps* was 42 mg O_2/hour[2,3]. Therefore (and rather unsurprisingly), the resting *N. coriiceps* can deliver more than enough oxygen to support its metabolic needs (main text, **Table 1**).

S1.1.2 Loss of Hb hinders O_2 delivery to tissue

Also, predictably, removing Hb and changing the O_2 transportation properties of the blood of *N. coriiceps* to match those of *C. aceratus* has catastrophic results for the test-fish. At 0.0067 mL O_2/mL blood[S7], BL_{O2} is an order of magnitude lower without hemoglobin. Accordingly, only 37 mg O_2/hour reaches the tissue, clearly not sufficient to support the resting VO_2 of *N. coriiceps* and low enough to challenge even *C. aceratus*, whose resting VO_2 has been measured between 24 and 45 mg O_2/hour (main text, **Table 1**)[S2-S4].

S1.1.3 Icefish adaptations rescue O2 delivery

One important way icefish combat the low oxygen carrying capacity of their blood is by increasing cardiac output. Raising Q of our test-fish to 7,140 mL blood/hour, matching that of *C. aceratus*[S9], increases O_2 delivery to 68 mg O_2/hour, enough to support the *N. coriiceps* VO_2 of 42 mg O_2/hour, but still substantially less than the 330 mg O_2/hour the fish achieves with normal cardiac output and oxygen solubility (main text, **Table 1**).

Beyond increased cardiac output, members of *Channicthyidae* have also been shown to be capable of a significant amount of gas exchange across their skin. One study estimated that cutaneous respiration could account for approximately 40% of *C. aceratus*' oxygen uptake, partially due to its lack of scales[S4,S10]. Surprisingly, *C. aceratus*' mass is nearly an order of magnitude larger than most other animals that exhibit similar percentage levels of cutaneous respiration[S8,S11]. Since *C. aceratus*' large size implies a lower surface-area-to-volume ratio, we would expect lower percentage levels of dermal gas exchange. Instead, these high levels indicate that skin breathing is another way the fish copes with a lack of Hb. Including this new level of cutaneous respiration in the list of adaptations for our test-fish, we find that it can deliver 78 mg O_2/hour which is still small, but at least approaches the same order of magnitude for *N. coriiceps* (main text, **Table 1**).

This level of cutaneous respiration corresponds to an oxygen permeability of ~1×10^{-11} mol/m/s/mmHg for *Channichthyidae* skin (calculated from several sources, details in **Supplementary Information S1.2**)[S3,S4,S12], the same order of magnitude as the 3.8×10^{-11} mol/m/s/mmHg reported for polydimethylsiloxane (PDMS)[S13], an elastomer common to microfluidics. Intriguingly, the use of gas-permeable PDMS devices to ensure proper oxygen delivery to tissues in a microfabricated HOC may have precedent in nature.

C. aceratus's ability to compensate for the low O_2 carrying capacity of its blood indicate that our own efforts to tune the O_2 carrying capacity of an HOC blood surrogate, or lack of a Hb analog therein, do not doom such efforts *ex ante*. This short exercise shows that Nature herself occasionally employs "engineering workarounds" and that extra-normal physiological values may be compensated by adjusting other parameters. In this case, two (carefully considered) wrongs *can* make a right. Further, *C. aceratus* demonstrates the value of introducing decoupling or redundant mechanisms to control important physiological parameters (e.g. vascular and cutaneous gas exchange to control O_2 delivery). These changes are not only useful for overcoming maladaptation, but also give designers a broader parameter space that can be used to achieve physiological relevance.

S1.2 *Calculation of C. aceratus skin permeability*

The following steps were used to calculate the permeability of *C. aceratus*' skin to molecular oxygen. The equation

$$N * A = P/L (C_o - C_i)$$

describes transport of gas across a barrier[S14] where:

N = molar flow O_2 [mol O_2/sec]
= ~10 mg O_2/h for a 1 kg *C. aceratus*[S4]

$= 0.00278$ mg O_2/s
$= 8.68 \times 10^{-8}$ mol O_2/s

A = fish surface area [m^2]
$= 1{,}892$ cm^2 for a 1 kg *C. aceratus*[S15]
$= 0.1892$ m^2

L = fish skin thickness [m]
= ~0.7 mm averaged between sensory line and lateral line values for *C. aceratus*[S12]
$= 7 \times 10^{-4}$ m

C_o = ocean ppO_2 [mmHg]
$= 150$ mmHg

C_i = *C. aceratus* blood ppO_2 [mmHg]
$= 120$ mmHg from[S3]

P = permeability of *C. aceratus* skin to oxygen

$$P = \frac{NL}{A(C_o - C_i)}$$

$$= 1.07 \times 10^{-11} \text{ mol } O_2 * \text{m}/\text{m}^2/\text{s}/\text{mmHg}$$

compared with 3.79×10^{-11} mol O_2/m/s/mmHg for PDMS[S13].

S1.3 *Further details on icefish blood volume*

S1.3.1 Comparison of blood volume as a function of body size

In addition to larger-than-expected cardiac output (mediated by a larger heart mass-body mass ratio)[S16], *C. aceratus* also has a blood volume of ~90 mL/kg, nearly twofold greater than the ~50 mL/kg predicted for a fish its size[S4,S17-S20]. Another member of *Channichthyidae*, *C. hamatus*, has a blood volume over two-fold its predicted value[S17]. These Hb– fish significantly exceed the blood volume expected from conventional quarter-powered scaling relationships (QPSRs) yet manage to function and flourish (**Supplementary Table 1**). Importantly, this observation reinforces the idea that extra-normal parameters can be an acceptable mechanism to thrive in the face of surprising physiology.

S1.3.2 Energy cost associated with increased blood volume

The increased blood volume shown in certain Hb– *Channichthyidae* species means that *C. aceratus*' heart must exert more energy to circulate that volume, especially at the high cardiac output required to maintain tissue oxygen levels. Researchers have estimated that *C. aceratus* allocates over one-fifth of its energy to driving circulation and that such a cost tradeoff offsets any gains in energy conservation made as a result of lower blood viscosity due to the loss of hemoglobin[S9,S10]. While this increased energy demand for circulation (driven mostly by a larger stroke volume rather than a faster heart beat) is certainly a concern for *C. aceratus*[S3,S9,S24], it could easily be addressed in an *in-vitro* system with the use of external assist devices, such as pumps[S25–S27], to make up for the energy deficit imparted by elevated blood volumes.

Supplementary Table 1 Expected and actual blood volumes in several *Notothenioidei*. In addition to the two fish considered in the bulk of this study, another species of icefish, *C. hamatus,* has been included to illustrate a second example of elevated blood volumes in *Channichthyidae*. Scaled values for macro and $\times 10^{-6}$ miniaturized humans are also included.

Organism	Mass/g	Blood volume/mL	
		Expected[a]	Observed
N. coriiceps	900	55	57[S20]
C. aceratus	1,400	85	126[S17]
C. hamatus	360	21	46[S17]
Human	70×10^3	4.3×10^3	5.9×10^3 [S21]
$\times 10^{-6}$ Human	0.07	0.006	—
$\times 10^{-6}$ HOC	0.07	0.006	0.06

[a] Values calculated from Refs. S22 and S23.

S1.3.3 Increased vascular density and vessel bore diameter

Observations of increased vascular density in *C. aceratus*[S28], made in retinal tissue, stand in contrast to other studies of icefish muscle that found decreased capillary density[S24,S29]. These muscle studies, however, also noted larger muscle fiber size in Hb– *Channichthyidae* compared to their Hb+ cousins. One group observed that such an increase in size would also decrease the rate of current leak from the muscle, conserving a substantial amount of energy and thereby decreasing the metabolic demand of the tissue[S29]. Therefore, measurements made in the retina, where no special adaptations (other than increased capillary density, of course) have been observed and oxygen demand is largely activity-level agnostic, may be a more faithful representation of the overall character of the fish. Furthermore, the large vessel diameters observed in *C. aceratus* may be explained by constitutive overexpression of NO, a potent vasodilator[S19,S28]. Since Hb-derivatives are involved in the major pathway for NO elimination[S30], their absence explains this overexpression and dictates that capillary diameter may not deviate as sharply from values predicted by scaling theory as initial reports indicate[S22,S23,S28,S31]. In an HOC, NO elimination in the absence of Hb may be achieved by incorporating PDMS, which is highly permeable to gases[S13], as well as taking advantage of the greater solubility of NO in liquid[S32].

S1.4 *Comparison of oxygen tissue penetration between Hb+ and Hb– Antarctic fish*

To model how the tissue penetration of oxygen may vary between *C. aceratus* and its Hb– cousin, *N. coriiceps*, we start with Equation (1) from the main text, describing the perfusion-limited diffusion of molecules from blood into tissue:

$$D \cdot \nabla^2 C = R,$$

where D = diffusion coefficient,
C = concentration of oxygen and
R = uptake of oxygen by tissue, governed by Michaelis–Menten kinetics.

In the special case of one-dimensional diffusion, the equation simplifies to:

$$\delta^2 / \delta x^2 \, C = \frac{\Omega * \gamma * C}{D * (K_M + C)},$$

where Ω = O_2 consumption per cell,
γ = cell density *in vivo* and
K_M = Michaelis constant.

The above equation was solved numerically using MatLab and the parameters described in **Supplementary Table 2** for the case of a Hb– Antarctic fish (*C. aceratus*) and an Hb+ Antarctic fish (*N. coriiceps*). By setting sufficiently positive and negative x-values equal to the boundary condition, C_C, we achieve the two boundary conditions necessary to solve the equation. The resulting solution is cut in half about the y-axis and a lower threshold of 2×10^{-2} mol $O_2 \cdot m^{-3}$ is imposed to represent the limit of cellular function[S33].

S2. Full derivation of distribution-informed approach to HOC blood volume

Starting from Equation (2) of the main text, we derive the relationship expressed in Equation (6) in full. A crude approximation of distribution for a perfusion-limited drug with low serum protein binding may assume partitioning to one of two compartments: body tissue or body water. This

Supplementary Table 2 Parameters used in solving Equation (1) of the main text for two different scenarios of an Hb+ Antarctic fish (*N. coriiceps*) and an Hb– Antarctic fish (*C. aceratus*).

Scenario	Parameter	Value	Notes	Source
Hb– (*C. aceratus*)	Ω, O_2 consumption per cell	5×10^{-18} mol $O_2 \cdot sec^{-1} \cdot cell^{-1}$	Reduced by 10× to account for lower BMR *in vivo*	S33
	γ, cell density	5×10^{14} cell $\cdot m^{-3}$	—	S34
	K_M, Michaelis constant	7.93×10^{-3} mol $O_2 \cdot m^{-3}$	—	S33
	C_C, capillary O_2 (boundary condition)	0.3 mol $O_2 \cdot m^{-3}$	—	S7
	D, diffusion coefficient of O_2 in tissue	1×10^{-9} $m^2 \cdot s^{-1}$	—	S33
Hb+ (*N. coriiceps*)	Ω, O_2 consumption per cell	7×10^{-18} mol $O_2 \cdot sec^{-1} \cdot cell^{-1}$	Adjusted up from Hb+ value by 40% to account for higher *N. coriiceps* metabolism	S33
	γ, cell density	5×10^{14} cell $\cdot m^{-3}$	—	S34
	K_M, Michaelis constant	7.93×10^{-3} mol $O_2 \cdot m^{-3}$	—	S33
	C_C, capillary O_2 (boundary condition)	1.3 mol $O_2 \cdot m^{-3}$	Taken to be half of maximum blood O_2 value reported	S7
	D, diffusion coefficient of O_2 in tissue	1×10^{-9} $m^2 \cdot s^{-1}$	—	S33

relationship can be expressed as a ratio of concentrations, also called a partition coefficient, K.

$$K = \frac{C_T}{C_W},$$

where K = partition coefficient,
C_T = concentration of drug in body tissue and
C_W = concentration of drug in body water.

Ignoring excretion and metabolism and devolving the concentration terms to amount over volume we obtain

$$K = \frac{(Dose - X_W)/V_T}{X_W/V_W},$$

where $Dose$ = total amount of drug administered,
X_W = total amount of drug in body water,
V_T = volume of body tissue, and
V_W = volume of body water.

Assuming no difference in concentration between blood and extracellular water, we rearrange to eventually arrive at Equation (5) of the main text

$$K = \frac{Dose * V_W}{V_T * X_W} - \frac{X_W * V_W}{V_T * X_W}$$

$$K + \frac{X_W * V_W}{V_T * X_W} = \frac{Dose}{V_T * C_B}$$

$$C_B = \frac{Dose}{\frac{X_W * V_W}{X_W} + K * V_T}$$

$$C_B = \frac{Dose}{(V_O + V_B) + K * V_T}$$

where V_B = blood volume,
V_O = non-blood body water volume and
C_B = concentration of drug in the blood = C_W = concentration of drug in body water.

Allowing blood volume to vary by an arbitrary multiple, Z, we obtain

$$C_B = \frac{Dose}{(V_O + Z * V_B) + K * V_T},$$

where Z = arbitrary blood volume multiplier.

Normalizing the result to a standard condition of $Z = 1$, we derive an expression for the normalized blood concentration of a small molecule drug of distribution coefficient, D, in the face changing blood volumes, Equation (6) of the main text:

$$C_B / C_{B0} = \frac{(V_o + V_B) + K * V_T}{(V_o + Z * V_B) + K * V_T},$$

where C_{B0} = concentration of the drug in blood for $Z = 1$.

S3. Other pharmacokinetic approaches to compensate for high HOC blood volumes for perfusion/transport limited substances

Classical pharmacokinetic/pharmacodynamics (PKPD) models address inter-organ interactions by using rate constants to account for mass transfer between different compartments that may effectively capture clinical behavior but have little physiological significance. Physiologically-based (PB-PKPD) models explicitly define blood flow as the medium by which analytes move between compartments[S35]. Although PBPK/PD models (also referred to as 'flow models') require extensive information about flow rates, compartment volumes and reaction rates, they also require less data fitting, are better able to accommodate pathological conditions, and are more easily extrapolated to describe PKPD behavior across species[S36].

In **Section 3** of the main text, we explored one way in which specific drug properties could be used to improve the efficacy of our HOC with super-physiologic blood volume (or estimate the error introduced by such an approach). Here, we further examine PB-PKPD approaches to mitigate any residual mismatch between HOC drug concentration levels and those that may occur in the body. We sketch out approaches to maintain steady state tissue concentration in the face of first order (**Supplementary Information S3.1**) and Michaelis–Menten reaction kinetics (**Supplementary Information S3.2**), as well as techniques to hold half-life (**Supplementary Information S3.3**) and area under the curve (**Supplementary Information S3.4**) constant from human to HOC. It should be noted that each of these approaches comes with its own set of caveats. For example, area under the curve (AUC) can be a useful metric for assessing total exposure, but can also mislead when different exposure profiles have the same AUC value but fall below or exceed certain critical thresholds such as minimum effective concentration or minimum toxic concentration.

S3.1 *PB-PKPD treatment to maintain steady-state tissue concentration with 1st-order kinetics*

PB-PKPD approaches typically idealize individual organ compartments as continuous-stirred tank reactors (CSTRs) where mixing times are

negligible and the concentration of a solute in the compartment is equal to the concentration of the outflow[S37–S39]. Assuming first-order reaction kinetics where the rate of reaction depends linearly on the concentration of the solute of interest within the compartment, as has been described previously[S39], we begin with the mass (or molar) balance for a particular solute in the tissue compartment:

$$dX_T/dt = Q_T * C_O - Q_T/K_T \; X_T/V_T - k * N_{Cells} \; X_T/V_T,$$

which describes the mass balance of a CSTR-idealized organ compartment where:

C_O = concentration of solute in the blood,
X_T = amount of solute in the organ/tissue compartment,
V_T = volume of the tissue compartment,
k = per cell first-order reaction rate constant (+ indicates consumption),
Q_T = tissue compartment flow rate,
N_{Cells} = number of cells in tissue compartment and
K_T = partition coefficient between the tissue and blood.

Assuming steady state ($dX_T/dt \rightarrow 0$) and replacing X_T/V_T with $C_{T\text{-}SS}$, the steady-state concentration in the tissue compartment, we obtain:

$$Q_T * C_O = C_{T-SS}\left(\frac{Q_T}{K_T} + k * N_{Cells}\right).$$

Solving for $C_{T\text{-}SS}$ yields the following:

$$C_{T-SS} = \frac{Q_T * C_O}{Q_T/K_T + k * N_{Cells}}.$$

We now reduce the blood concentration, C_O, by a blood volume increase induced dilution factor, J (which can be estimated from the distribution-based treatment outlined in **Section 3** in the main text and **Supplementary Information S2**, for example, in the face of a 10× blood volume increase, $J = 2.28$ for epinephrine, $J = 1.06$ for propranolol and $J = 1$ for amiodarone), and introduce a new tissue flow rate, P_T:

$$C_{T-SS} = \frac{P_T C_O/J}{P_T/K_T + k * N_{Cells}},$$

where J = dilution factor induced by blood volume increase, depending on both drug properties (D) and magnitude of blood volume increase (Z).

Since we wish to maintain $C_{T\text{-}SS}$ across both scenarios, we set the two preceding equations equal and solve for P_T, yielding:

$$P_T = \frac{J * Q_T * N_{Cells} * k}{N_{Cells} * k - (J-1)\,Q_T/K_T}.$$

Therefore, if fractional flow rates to each organ and other relevant parameters are maintained, a new system flow rate (cardiac output) can be selected to maintain steady-state tissue level of a *specific* drug. This approach may be especially useful if another method (e.g. incorporation of gas permeable materials such as PDMS) is used to decouple oxygen delivery from blood flow.

S3.2 *PB-PKPD treatment to maintain steady-state tissue concentration with Michaelis–Menten kinetics*

A more complicated, but perhaps more realistic, treatment involves assuming Michaelis–Menten reaction kinetics in the organ compartment. We note that Michaelis–Menten kinetics have previously been used to numerically model oxygen consumption within a bioreactor[S33] as well as toxicity of an anti-cancer drug in a three-organ HOC[S38]. Starting with the mass balance:

$$dX_T/dt = Q_T C_O - Q_T/K_T \; X_T/V_T - \frac{V_{Max} \, X_T/V_T}{K_M + X_T/V_T} N_{Cells},$$

which describes the mass balance of a CSTR-idealized organ compartment where:

C_O = concentration of solute in the blood,
X_T = amount of solute in the tissue/organ compartment,
V_T = volume of the tissue compartment,
V_{Max} = maximum per cell reaction rate,
K_M = the Michaelis constant,
Q_T = tissue compartment flow rate,
N_{Cells} = number of cells in compartment and
K_T = partition coefficient between the tissue and blood.

Assuming steady state ($dX_T/dt \rightarrow 0$) and replacing X_T/V_T with $C_{T\text{-}SS}$, the steady-state concentration in the tissue compartment, we obtain:

$$Q_T C_O = C_{T-SS} \, Q_T/K_T + N_{Cells} \frac{V_{Max} C_{T-SS}}{K_M + C_{T-SS}}.$$

Expanding and collecting terms gives:

$$0 = C_{T-SS}^2\left(Q_T/K_T\right) + C_{T-SS}^1\left(K_M \, Q_T/K_T - V_{Max} - Q_T C_O\right) + C_{T-SS}^0\left(K_M Q_T C_O\right).$$

Using the quadratic formula to solve for C_{T-SS} yields:

$$C_{T-SS} = \frac{Q_T C_O + V_{Max} - K_M \frac{Q_T}{K_T} \pm \sqrt{\left(K_M \frac{Q_T}{K_T} - V_{Max} - Q_T C_O\right)^2 - 4\frac{Q_T}{K_T}\left(K_M Q_T C_O\right)}}{2\,Q_T/K_T}.$$

At this point the analytical treatment becomes quite cumbersome. The interested reader may obtain a solution for an adjusted flow rate, P_T, as in **Supplementary Information S3.1**, or may instead choose to solve the problem numerically as done previously[S33,S38].

S3.3 *PB-PKPD treatment to maintain half-life*

Drug half-life is another important parameter that concerns pharmacologists[S40]. Half-life, HL, can be described by the following equation:

$$HL = \frac{0.693 K_P}{Q/V},$$

where Q = flow rate,
V = compartment volume and
K_P = equilibrium partition coefficient.

Therefore, half-life is unaffected by changes in blood volume.

S3.4 *PBPK/PD treatment to maintain AUC*

AUC is a common metric for assessing patient dose[S41–S43]. For example, if the clearance of a drug and its metabolites can be assumed to be perfusion limited — that is the rate of clearance from the bloodstream is much greater than the rate of delivery to clearing organ — decreasing the cardiac output will increase the AUC (or vice versa)[S44]:

$$AUC = \frac{X}{F_{CL} * Q}$$

where X = the amount of drug administered in mg or moles,
F_{Cl} = clearance fraction of drug and
Q = cardiac output.

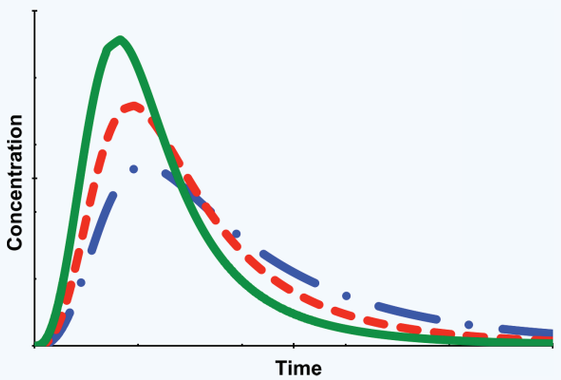

Supplementary Figure 1 Three arterial concentration curves with different cardiac output–dose parameters but identical AUC's demonstrating how engineering controls can be used to maintain a target exposure profile in the face of challenges associated with miniaturization. Computed using PKQuest software from Refs. S45 and S46 and data from Ref. S47.

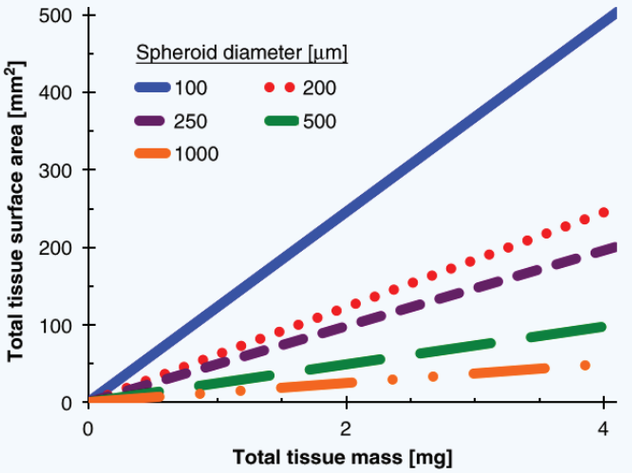

Supplementary Figure 2 Cell-dense 3D tissue constructs (spheroids) can control the relationship between tissue surface area and volume. Depending on spheroid diameter, different surface area–volume curves may be obtained.

Thus, even in the face of increased dosing as proposed above, engineering modifications can be used to maintain other important pharmacokinetic parameters such as AUC. Using the open-source PKQuest PBPK modeling software we can examine how dose and cardiac output may be manipulated to preserve AUC (**Supplementary Fig. 1**)[S45–S47]. Critically, uncoupling these and other parameters — as we have begun to attempt here — will offer technologists multiple axes along which to tune exposure profiles and represents one potential solution to overcoming the substantial engineering challenges of developing a micro-scale model of the human body.

S4. Surface area–mass considerations for 3D constructs in an HOC system

Three-dimensional (3D) tissue constructs can lead to improved phenotype and function *in-vitro* for a variety of cell types, including liver cells[S48]. Using 3D aggregates also introduces a more complicated relationship between mass and surface area. For this reason, spheroid size and number must be carefully considered during design. Below is a graph representing the relationship between HOC organ mass and surface area for spheroids of various sizes (**Supplementary Fig. 2**). Since spheroids of diameter 250 µm have been shown to exhibit highest levels of liver specific function (unpublished data), the dashed, purple curve is used to inform our design process.

S5. Other HOC design-related tables

S5.1 *Comparison between ×10^{-6} HOC and a macro- and micro-human*

We can compare the organ- and system-level parameters for our ×10^{-6} HOC (**Table 3** of the main text) to actual values of a macro-human and

Supplementary Table 3 Comparison of relevant design parameters between a "macro" (life-size) human and the ×10^{-6} HOC proposed here.

Organ		Macro-Human			×10^{-6} HOC				
		Surface area [m^2]	Tissue Mass [kg]	% CO	Surface area [mm^2]	Tissue mass [mg]	Blood volume (BV) [µL]	% CO	% BV
Lung	*Endothelium*	*30*	—	—	*30*	*0.12*	*1.1*	—	—
	Non-EC	*40*	—	—	*40*	*0.16*	*1.4*	—	—
	Total	70	0.47	100	70	0.28	2.5	100	4
Liver	*Endothelium*	*80*	*0.3*	—	*80*	*0.32*	*2*	—	—
	Non-EC	*320*	*1.2*	—	*34*	*1.75*	*1.03*	—	—
	Total	400	1.5	25	114	2.07	3.03	25	5
Heart		—	0.33	4	—	0.33	0.28	4	0.5
Fat		—	12.5	5	—	12.5	10.7	5	18
Blood		—	—	—	—	—	18	—	—
"Other tissues"		—	—	—	—	48.8	43.5	66	73
Blood Oxygen Content [BL_{O2}; mol O_2/m^3]		7			~2				
Cutaneous Respiration [mol/m/s/mmHg]		3.5×10^{-12}			$\leq 3.8 \times 10^{-11}$				
Cardiac Output [mL/s]		110			3.4×10^{-3}				
Intervessel Distance [IVD; µm]		300			250				

Supplementary Table 4 Comparison of relevant design parameters for two of HOCs ($\times10^{-4}$ and $\times10^{-7}$) are presented here.

Organ		Micro (10^{-6})-Human				$\times10^{-6}$ HOC			
		Surface area [mm^2]	Tissue mass [mg]	Blood volume (BV) [μL]	% BV	Surface area [mm^2]	Tissue mass [mg]	Blood volume [μL]	% BV
Lung	*Endothelium*	*30*	—	—	—	*30*	*0.12*	*1.1*	—
	Non-EC	*40*	—	—	—	*40*	*0.16*	*1.4*	—
	Total	70	0.47	2.5	42	70	0.28	2.5	4
Liver	*Endothelium*	*80*	*0.3*	—	—	*80*	*0.32*	*2*	—
	Non-EC	*320*	*1.2*	—	—	*34*	*1.75*	*1.03*	—
	Total	400	1.5	3.03	51	114	2.07	3.03	5
Heart		—	0.33	0.28	4.7	—	0.33	0.28	0.5
Fat		—	12.5	10.7	178	—	12.5	10.7	18
Blood		—	—	6	—	—	—	60	—
"Other Tissues"		—	48.8	43.5	725	—	48.8	43.5	73
Blood Oxygen Content [BL_{O2}; mol O_2/m^3]		7				~2			
Cutaneous Respiration [mol/m/s/mmHg]		3.5×10^{-12}				$\leq 3.8 \times 10^{-11}$			
Cardiac Output [mL/s]		3.4×10^{-3}				3.4×10^{-3}			
Intervessel Distance [IVD; μm]		87				250			

Supplementary Table 5 Complete design parameters for a $\times10^{-4}$ HOC.

Organ		Class	$\times10^{-4}$ HOC							
			Surface area [mm^2]	Tissue mass [mg]	Blood volume (BV) [μL]	% BV	% CO	Compartment dimension		
								Length [mm]	Width [mm]	Height [mm]
Lung	*Endothelium*	*F-2D*	3×10^3	*11.9*	*105*	—	—	—	—	—
	Non-EC	*F-2D*	4×10^3	*15.9*	*140*	—	—	—	—	—
	Total	F-2D	7×10^3	27.9	245	4	100	29	245	0.035
Liver	*Endothelium*	*F-2D*	8×10^3	*31.8*	*200*	—	—	*47*	*170*	*0.025*
	Non-EC	*F-3D*	3.4×10^3	*175*	*102*	—	—	*25*	*20*	*1*
	Total	F-2/3D	11×10^3	206	302	5	25	—	—	—
Heart		F-3D	—	33	28	0.5	4	10.6	10.6	0.5
Fat		F-3D	—	1.3×10^3	1071	18	5	50	50	1
Blood		—	—	—	6×10^3	—	—	—	—	—
"Other Tissues"		F-3D	—	4.8×10^3	4.4×10^3	73	66	66	66	1
Blood Oxygen Content [BL_{O2}; mol O_2/m^3]			~2							
Cutaneous Respiration [mol/m/s/mmHg]			$\leq 3.8 \times 10^{-11}$							
Cardiac Output [mL/s]			1.07×10^{-1}							
Intervessel Distance [IVD; μm]			250							

values predicted by QPSR for a mini-human. Like **Fig. 7** of the main text, these comparisons highlight ways in which our HOC design departs from known or predicted values.

S5.2 *Design parameters for HOCs of other sizes*

For convenience and completeness, design parameters for two other HOCs ($\times10^{-4}$ and $\times10^{-7}$) are presented here.

S6. Derivation of design radar charts

S6.1 *Creation of radar charts*

To create radar graphs of **Fig. 7** of the main text for human, mouse, icefish and $\times10^{-6}$ HOC, observed values were normalized against scaling values and plotted along five $\log_{10}$ axes in Microsoft Excel.

S6.2 *C. aceratus radar chart normalized against N. coriiceps*

Since *C. aceratus* is poikilothermic, metabolic values for the fish are likely substantially affected by ambient temperature. Although several correction factors have been proposed to compare cold-water fish to animals with warmer body temperatures[S55,S56], no reliable method exists to adjust all relevant parameters considered here. One way to circumvent this problem is to normalize *C. aceratus* to another fish from the same environment that can be assumed to follow conventional scaling laws that describe most of the rest of the natural world. For completeness, this chart for *C. aceratus* normalized against *N. coriiceps* is included here (**Supplementary Fig. 3**).

Supplementary Table 6 Complete design parameters for a $\times 10^{-7}$ HOC.

Organ		Class	$\times 10^{-7}$ HOC							
			Surface area [mm^2]	Tissue mass [mg]	Blood volume (BV) [μL]	% BV	% CO	Compartment dimension		
								Length [mm]	Width [mm]	Height [mm]
Lung	*Endothelium*	*F-2D*	*3*	*0.012*	*0.11*	—	—	—	—	—
	Non-EC	*F-2D*	*4*	*0.016*	*0.14*	—	—	—	—	—
	Total	F-2D	7	0.028	0.25	4	100	5.07	1.38	0.035
Liver	*Endothelium*	*F-2D*	*8*	*0.032*	*0.2*	—	—	8.36	0.96	0.025
	Non-EC	*F-3D*	*3.44*	*0.175*	*0.1*	—	—	0.5	0.5	1
	Total	F-2/3D	11.4	0.207	0.3	5	25	—	—	—
Heart		F-3D	—	0.033	0.028	0.5	4	0.33	0.33	0.5
Fat		F-3D	—	1.25	1.07	18	5	1.6	1.6	1
Blood		—	—	—	6	—	—	—	—	—
"Other Tissues"		F-3D	—	4.88	4.35	73	66	2.09	2.09	1
Blood Oxygen Content [BL_{O2}; mol O_2/m^3]										~2
Cutaneous Respiration [mol/m/s/mmHg]										$\leq 3.8 \times 10^{-11}$
Cardiac Output [mL/s]										6.04×10^{-4}
Intervessel Distance [IVD; μm]										250

Supplementary Table 7 Table of observed values (with sources).

	Blood O2 [mol O_2/m^3]	Blood volume [mL]	Cardiac output [mL/s]	Cutaneous respiration [mol/m/s/mmHg]	Intervessel distance [IVD; μm]
C. aceratus	0.3[S7]	125[S17]	2[S9]	1×10^{-11} [S4]	293[S28]
N. coriiceps	2.7[S7]	55[S20]	1[S49]	3.5×10^{-12} [S50]	646[S28]
Human	7[S30]	5,900[S21]	112[S21]	3.5×10^{-12} [S50]	200[S51]
$\times 10^{-6}$ HOC	~2 (α)	0.06 (β)	3.4×10^{-3} (γ)	3.8×10^{-11} [S13]	250 (δ)
Mouse	5.95[S52]	2[S26]	0.27[S53]	3.5×10^{-12} [S50]	180[S54]

α – Design consideration to induce *in-vivo*-like cellular BMR (see Section 2 of main text).
β – Design consideration arrived at by applying QPSR isometric scaling of blood volume to miniaturize human by six orders of magnitude. The resulting value (6 μL) is adjusted upwards by a factor of 10 to achieve a more workable volume.
γ – Design consideration arrived at by applying QPSR ¾-power scaling of cardiac output to a $\times 10^{-6}$ miniaturized human.
δ – Design consideration to accommodate liver spheroids of 250 μm in diameter.

Supplementary Table 8 Table of scaling values (calculated from scaling laws).

	Mass [kg]	Blood O_2 [mol O_2/m^3] (ε)	Blood volume [mL] (ζ)	Cardiac output [mL/s] (η)	Cutaneous respiration [mol/m/s/mmHg] (θ)	Intervessel distance [IVD; μm] (ι)
C. aceratus	1	6.5	60.9	4.44	3.5×10^{-12}	186
N. coriiceps	1	6.5	60.9	4.44	3.5×10^{-12}	186
Human	70	6.5	4263	107.4	3.5×10^{-12}	265
$\times 10^{-6}$ HOC	7×10^{-5}	6.5	6×10^{-3}	3.4×10^{-3}	3.5×10^{-12}	87
Mouse	0.03	6.5	1.83	0.32	3.5×10^{-12}	139

ε – Assumed to be mass invariant (μM^0) for Hb+ vertebrates.
ζ – Calculated per the equation $Y = 60.9 * M^1$. Exponent selected according to scaling law and coefficient taken as average of four values reported in Ref. S23.
η – Calculated per the equation $Y = 4.44 * M^{0.75}$. Exponent selected according to scaling law and coefficient taken as average of two values reported in Ref. S23.
θ – No scaling value known. Permeability of human skin used for all values[S50].
ι – Calculated per the equation $Y = 186 * M^{0.083}$. Exponent selected according to scaling law and, since no literature value could be found, coefficient selected to give reasonable match to mouse and human values[S22].

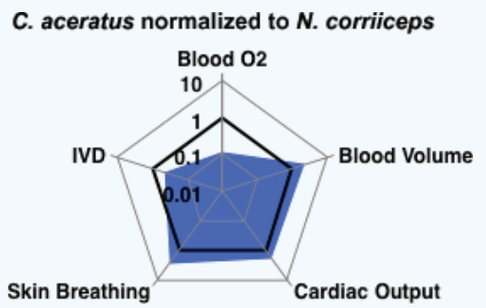

Supplementary Figure 3 Radar chart of *C. aceratus* normalized to its cousin, *N. coriiceps* instead of conventional parameters predicted by quarter power scaling relationships.

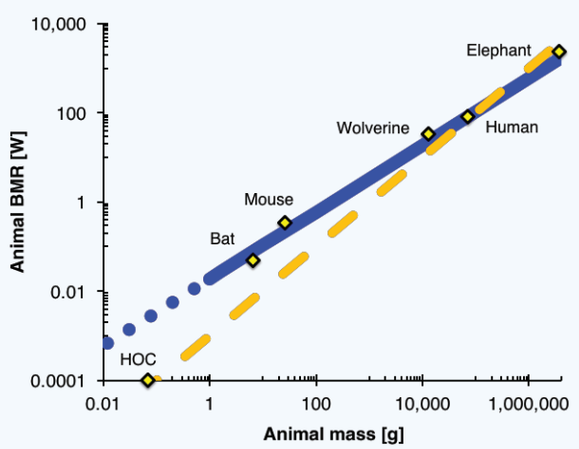

Supplementary Figure 4 Metabolically-supported scaling posits that designers must control cellular BMR in order to achieve a generalizable, *in-vivo*-like response from a miniaturized experimental system. A consequence of matching *in-vitro* cellular BMR to *in-vivo* levels is that system BMR scales as M^1.

S7. Explanation of M1 scaling for F-2D and F-3D organs

An interesting consequence of this strategy is that, by virtue of holding cell BMR constant, it abolishes the $M^{3/4}$ dependence of system BMR, instead replacing it with an M^1 dependence and causing the relationship between human and HOC system BMR to lie on a fundamentally different trajectory than human-animal (**Supplementary Fig. 4**). This explains why both F-2D and F-3D organs are scaled as M^1.

REFERENCES

S1. FishBase. *Notothenia coriiceps* (2005), http://www.fishbase.se/Photos/PicturesSummary.php?ID=4702&what=species
S2. Ralph, R. & Everson, I. The respiratory metabolism of some Antarctic fish. *Comp. Biochem. Physiol.* **27**, 299–307 (1968).
S3. Holeton, G.F. Oxygen uptake and circulation by a hemoglobinless Antarctic fish (*Chaenocephalus aceratus* Lonnberg) compared with three red-blooded Antartic fish. *Comp. Biochem. Physiol.* **34**(2), 457–471 (1970).
S4. Hemmingsen, E.A. & Douglas, E.L. Respiratory characteristics of the hemoglobin-free fish *Chaenocephalus aceratus*. *Comp. Biochem. Physiol.* **33**(4), 733–744 (1970).
S5. Egginton, S. Control of tissue blood flow at very low temperatures. *J. Therm. Biol.* **22**(6), 403–407 (1997).
S6. Feder, M.E. & Burggren, W.W. Cutaneous gas exchange in vertebrates: Design, patterns, control and implications. *Biol. Rev.* **60**(1), 1–45 (1985).
S7. Ruud, J.T. Vertebrates without erythrocytes and blood pigment. *Nature* **173**(4410), 848–850 (1954).
S8. Nonnotte, G. & Kirsch, R. Cutaneous respiration in seven sea-water teleosts. *Respir. Physiol.* **35**, 111–118 (1978).
S9. Hemmingsen, E.A., Douglas, E.L., Johansen, K. & Millard, R.W. Aortic blood flow and cardiac output in the hemoglobin-free fish *Chaenocephalus aceratus*. *Comp. Biochem. Physiol. A Physiol.* **43**(4), 1045–1051 (1972).
S10. Hemmingsen, E.A. Respiratory and cardiovascular adaptations in hemoglobin-free fish: Resolved and unresolved problems. In *Biology of Antarctic Fish* (ed.) di Prisco, G., Maresca, B. & Tota, B. (Springer, 1991), pp. 191–203.
S11. Kock, K.-H. Antarctic icefishes (Channichthyidae): A unique family of fishes. A review, Part I. *Polar. Biol.* **28**(11), 862–895 (2005).
S12. Walvig, F. The integument of the icefish *Chaenocephalus aceratus* (Lonnberg). *Nor. J. Zool.* **9**, 31–36 (1960).
S13. Brandrup, J., Immergut, E.H. & Grulke, E.A. *Polymer Handbook* (John Wiley & Sons, 1998).
S14. Bird, R.B., Stewart, W.E. & Lightfoot, E.N. *Transport Phenomena* (John Wiley & Sons, 2007).
S15. Holeton, G.F. Respiratory morphometrics of white and red blooded Antarctic fish. *Comp. Biochem. Physiol.* **54A**, 215–220 (1976).
S16. Tota, B., Acierno, R. & Agnisola, C. Mechanical performance of the isolated and perfused heart of the haemoglobinless Antarctic icefish *Chionodraco hamatus* (Lonnberg): Effects of loading conditions and temperature. *Philos. Trans. R. Soc. Lond. B Biol. Sci.* **332**(1264), 191–198 (1991).
S17. Acierno, R., MacDonald, J.A., Agnisola, C. & Tota, B. Blood volume in the hemoglobinless Antarctic teleost *Chionodraco hamatus* (Lönnberg). *J. Exp. Zool.* **272**(5), 407–409 (1995).
S18. Eastman, J.T. *Antarctic Fish Biology: Evolution in a Unique Environment* (Academic Press Limited, 1993).
S19. Sidell, B.D. & O'Brien, K.M. When bad things happen to good fish: The loss of hemoglobin and myoglobin expression in Antarctic icefishes. *J. Exp. Biol.* **209**(10), 1791–1802 (2006).
S20. Twelves, E.L. Blood volumes of two Antarctic fishes. *Antarct. Surv. Bull.* (31), 85–92 (1972).
S21. Williams, L.R. & Leggett, R.W. Reference values for resting blood flow to organs of man. *Clin. Phys. Physiol. Meas.* **10**(3), 187 (1989).
S22. West, G.B., Brown, J.H. & Enquist, B.J. A general model for the origin of allometric scaling laws in biology. *Science* **276**(5309), 122–126 (1997).
S23. Peters, R.H. *The Ecological Implications of Body Size* (Cambridge University Press, 1983).
S24. Fitch, N.A., Johnston, I.A. & Wood, R.E. Skeletal muscle capillary supply in a fish that lacks respiratory pigments. *Respir. Physiol.* **57**, 201–211 (1984).
S25. Moraes, C. *et al*. On being the right size: Scaling effects in designing a human-on-a-chip. *Integr. Biol.* **5**(9), 1149 (2013).
S26. Wikswo, J.P. *et al*. Engineering challenges for instrumenting and controlling integrated organ-on-chip systems. *IEEE Trans. Biomed. Eng.* **60**(3), 682–690 (2013).
S27. Wikswo, J.P. *et al*. Scaling and systems biology for integrating multiple organs-on-a-chip. *Lab Chip* **13**(18), 3496 (2013).
S28. Wujcik, J.M., Wang, G., Eastman, J.T. & Sidell, B.D. Morphometry of retinal vasculature in Antarctic fishes is dependent upon the level of hemoglobin in circulation. *J. Exp. Biol.* **210**(5), 815–824 (2007).
S29. O'Brien, K.M. Muscle fine structure may maintain the function of oxidative fibres in haemoglobinless Antarctic fishes. *J. Exp. Biol.* **206**(2), 411–421 (2003).
S30. Widmaier, E.P., Raff, H. & Strang, K.T. *Vander's Human Physiology* (McGraw-Hill, 2006).
S31. Banavar, J.R. *et al*. A general basis for quarter-power scaling in animals. *Proc. Natl. Acad. Sci. USA* **107**(36), 15816–15820 (2010).
S32. Weiss, R.F. & Price, B.A. Nitrous oxide solubility in water and seawater. *Mar. Chem.* **8**, 347–359 (1980).
S33. Mattei, G., Giusti, S. & Ahluwalia, A. Design criteria for generating physiologically relevant *in vitro* models in bioreactors. *Processes* **2**(3), 548–569 (2014).
S34. Bianconi, E. *et al*. An estimation of the number of cells in the human body. *Ann. Hum. Biol.* **40**(6), 463–471 (2013).
S35. Jones, H. & Rowland-Yeo, K. Basic concepts in physiologically based pharmacokinetic modeling in drug discovery and development. *CPT Pharmacomet. Syst. Pharmacol.* **2**(8), e63 (2013).
S36. Shargel, L. & Yu, A.B.C. *Applied Biopharmaceutics and Pharmacokinetics* (Appleton & Lange, 1993).
S37. Schmidt, L.D. *The Engineering of Chemical Reactions* (Oxford University Press, 1998).
S38. Sung, J.H., Kam, C. & Shuler, M.L. A microfluidic device for a pharmacokinetic–pharmacodynamic (PK–PD) model on a chip. *Lab Chip* **10**(4), 446 (2010).
S39. Abaci, H.E. & Shuler, M. Human-on-a-chip design strategies and principles for physiologically based pharmocokinetics/pharmacodynamics modeling. *Integr. Biol.* **7**(4), 383–391 (2015).
S40. Rowland, M. & Tozer, T.N. *Clinical Pharmacokinetics: Concepts and Applications* (Williams & Wilkins, 1995).

S41. U.S. Environmental Protection Agency. Approaches for the application of physiologically based pharmacokinetic (PBPK) models and supporting data in risk assessment (EPA, 2006), https://ofmpub.epa.gov/eims/eimscomm.getfile?p_download_id=458188
S42. Clewell III, H.J., Andersen, M.E. & Barton, H.A. A consistent approach for the application of pharmacokinetic modeling in cancer and noncancer risk assessment. *Environ. Health Perspect.* **110**(1), 85 (2002).
S43. Voisin, E.M., Ruthsatz, M., Collins, J.M. & Hoyle, P.C. Extrapolation of animal toxicity to humans: Interspecies comparisons in drug development. *Regul. Toxicol. Pharmacol.* **12**(2), 107–116 (1990).
S44. Upton, R.N., Ludbrook, G.L., Grant, C. & Martinez, A.M. Cardiac output is a determinant of the initial concentrations of propofol after short-infusion administration. *Anesth. Analg.* **89**(3), 545 (1999).
S45. Levitt, D.G. PKQuest: A general physiologically based pharmacokinetic model. Introduction and application to propranolol. *BMC Pharmacol. Toxicol.* **2**(1), 5 (2002).
S46. Levitt, D.G. PKQuest_Java: Free, interactive physiologically based pharmacokinetic software package and tutorial. *BMC Res. Notes* **2**(1), 158 (2009).
S47. Arancibia, A., Guttmann, J., Gonzalez, G. & Gonzalez, C. Absorption and disposition kinetics of amoxicillin in normal human subjects. *Antimicrob. Agents Chemother.* **17**(2), 199–202 (1980).
S48. Torisawa, Y. *et al*. A multicellular spheroid array to realize spheroid formation, culture, and viability assay on a chip. *Biomaterials* **28**(3), 559–566 (2007).
S49. Egginton, S. Blood rheology of Antarctic fishes: Viscosity adaptations at very low temperatures. *J. Fish Biol.* **48**(3), 513–521 (1996).
S50. Stücker, M. *et al*. The cutaneous uptake of atmospheric oxygen contributes significantly to the oxygen supply of human dermis and epidermis. *J. Physiol.* **538**(3), 985–994 (2002).
S51. Folarin, A.A., Konerding, M.A., Timonen, J., Nagl, S. & Pedley, R.B. Three-dimensional analysis of tumour vascular corrosion casts using stereoimaging and micro-computed tomography. *Microvasc. Res.* **80**(1), 89–98 (2010).
S52. Petschow, R., Petschow, D., Bartels, R., Baumann, R. & Bartels, H. Regulation of oxygen affinity in blood of fetal, newborn and adult mouse. *Respir. Physiol.* **35**(3), 271–282 (1978).
S53. Tournoux, F. *et al*. Validation of noninvasive measurements of cardiac output in mice using echocardiography. *J. Am. Soc. Echocardiogr.* **24**(4), 465–470 (2011).
S54. Malkusch, W., Konerding, M.A., Klapthor, B. & Bruch, J. A simple and accurate method for 3-D measurements in microcorrosion casts illustrated with tumour vascularization. *Anal. Cell. Pathol.* **9**(1), 69–81 (1995).
S55. Ege, R. & Krogh, A. On the relation between the temperature and the respiratory exchange in fishes. *Int. Rev. Gesamten. Hydrobiol. Hydrogr.* **7**(1), 48–55 (1914).
S56. Clarke, A. & Johnston, N.M. Scaling of metabolic rate wtih body mass and temperature in telost fish. *J. Anim. Ecol.* **68**, 893–905 (1999).